Cell-autonomous control coupled with tissue context regulates the cessation of migration at the site of organ development

Katsiaryna Tarbashevich[1,*], Zahra Labbaf[1,*], Moritz Ophaus[1], Jan Schick[1], Lucas Kühl[1], Sargon Gross-Thebing[1], Michal Reichman-Fried[1], Dennis Hoffmann[1], Martin Stehling[2], Jochen Seggewiss[3], Christian Ruckert[3], Johanna B. Kroll[4], Jan Philipp Junker[4,5], Erez Raz[1,2,‡]

[1]Institute of Cell Biology, ZMBE, Von-Esmarch-Straße 56, 48149 Muenster, Germany
[2]Max-Planck-Institute for Molecular Biomedicine, Roentgenstraße 20, 48149 Muenster, Germany
[3]Center for Medical Genetics, Clinic for Medical Genetics, University Hospital Muenster (UKM), University Muenster, Vesaliusweg 12-14, 48149 Muenster, Germany
[4]Max Delbrück Center for Molecular Medicine in the Helmholtz Association, Berlin Institute for Medical Systems Biology, Berlin, Germany
[5]Charité – Universitätsmedizin Berlin, Germany

[*]Contributed equally
[‡]Author for correspondence: erez.raz@uni-muenster.de

Keywords: zebrafish, primordial germ cell, cell migration, cell polarity, gonad, organogenesis, Dnd1

Abstract

Organ development relies on interactions among different cell types that form three-dimensional structures to carry out specific tasks. This process often involves active migration of progenitor cells toward specific positions within the embryo, where the cells then become immotile and form stable connections among themselves and with neighboring cells. In this work, we study the process of motility loss using zebrafish primordial germ cells as an *in vivo* model. We show that changes in embryonic tissues as well as cell-autonomous events regulate germ cells' behavior as they arrive at their target region. Importantly, we find that reduction in germ cell motility is correlated with the decay of RNA encoding for Dead end 1 (Dnd1), a conserved vertebrate RNA-binding protein that is essential for PGC migration. Indeed,

© 2026. Published by The Company of Biologists
This is an Open Access article distributed under the terms of the Creative Commons Attribution License (http://creativecommons.org/licenses/by/4.0), which permits unrestricted use, distribution and reproduction in any medium provided that the original work is properly attributed

decreasing or increasing the level of Dnd1 results in a premature or delayed stop to motility, respectively. These findings represent an RNA decay-based mechanism for timing the duration of cell migration *in vivo*.

Summary Statement

Migratory cells that participate in organ development lose motility upon arrival at their target. We present mechanisms governing this process during the early stages of gonad formation in zebrafish embryos.

Introduction

During organogenesis, progenitor cells often migrate toward specific positions within the embryo, where they stop and form stable connections with each other and with other cells and differentiate. Cessation of migration is controlled by mechanisms, such as contact inhibition of locomotion or activation of specific receptors that provide a stop signal (e.g. for migrating T-cells) (Molon et al., 2022; Roycroft and Mayor, 2016; Shellard and Mayor, 2019). In addition, the motility can be regulated by desensitization of the chemoattractant receptor (Coombs et al., 2019; Kienle et al., 2021; Minina et al., 2007) and differential adhesion ((Cortés et al., 2003), reviewed in (Miskolci et al., 2021; Yamaguchi and Knaut, 2022)).

A model for investigating the stop in migration in organogenesis *in vivo* is the gonad, because the progenitors of the germline, namely primordial germ cells (PGCs), often form away from the region where the gonad develops (Grimaldi and Raz, 2020). The chemokine Cxcl12 directs PGC migration as was first demonstrated in zebrafish (Doitsidou et al., 2002; Knaut et al., 2003; Schick et al., 2025) and then in other organisms (Nishiumi et al., 2005; Stebler et al., 2004; Takeuchi et al., 2010) (Herpin et al., 2008) (Ara et al., 2003; Molyneaux et al., 2003; Stebler et al., 2004). Zebrafish PGCs arrive at the gonad region, maintain motility, interact with somatic cells and structures in the area (Paksa et al., 2016), and eventually stop. In this work, we study the mechanisms of motility loss in PGCs during early gonadogenesis. We show that the maternally provided RNA encoding for the Dead end1 (Dnd1) protein functions as a “molecular clock” that controls the timing at which cell behavior

Development • Supplementary information

switches from a motile to an immotile phase, allowing PGCs to form stable connections to somatic cells and generate gametes.

Results and Discussion

Germ cell migration speed is reduced during development

To investigate the events occurring after PGCs reach the gonad region, we characterized cell behavior at 24 hours post fertilization (hpf), when most of them have reached the target area (Weidinger et al., 1999), as well as 12 hours later (36 hpf). At 24 hpf, the migration speed is about half of that observed for PGCs at 7-9 hpf (2 µm/min at the early stages (Reichman-Fried et al., 2004)). 12 hours later, it is lowered to about a quarter of its speed at 7-9 hpf (Fig. 1A, B). We also observed a strong decrease in displacement (Fig. S3B), which was reduced from 12 µm at 24-26 hpf to 4 µm at 34-36 hpf per 1 hour (Fig. 1A, C; Movie S1). Thus, by 36 hpf PGCs exhibit little movement at the gonad region. The behavior of PGC at the target site can be controlled by cell-extrinsic factors, such as specific chemical or physical cues at the target region (Doren and Lehmann, 1997; Paksa et al., 2016), and potentially by cell-autonomous mechanisms.

To investigate the role of possible cues within the gonad region in PGCs' loss of motility, we aimed to identify relevant genes expressed in somatic cells adjacent to PGCs at 24 hpf. To this end, we performed RNA tomography (tomo-seq) experiments (Junker et al., 2014). We sectioned embryos along the anterior-posterior or the dorsal-ventral axes and performed RNA sequencing on the individual tissue slices (Fig. S1A). This procedure provided us with a spatial RNA expression map of the gonad region.

Indeed, we could detect germ cell-expressed RNA molecules such as *ca15b* (Tarbashevich et al., 2015; Wang et al., 2013), *dnd1* (Weidinger et al., 2003), and *nos3* (Köprunner et al., 2001)). To identify genes with expression patterns similar to known PGC markers, we compared the spatial expression profiles to the germ cell marker *ddx4* (*vasa*). This analysis revealed that many genes expressed in the proximal convoluted tubule (PCT) segment of the pronephric duct (Wingert and Davidson, 2008) exhibited profiles similar to that of *vasa* (Fig. S1B, Table S1). *In situ*

Development • Supplementary information

hybridization experiments revealed that the PGCs were located ventral to the PCT (Fig. S2A, B).

To determine whether the interaction between PGCs and the PCT could affect PGCs' positioning, we ablated the PCT by expressing the bacterial toxin Kid within it, employing *UAS:kid* fish (*Tg(UAS:kid*), (Labbaf et al., 2022)) and fish expressing GAL4 and GFP in the PCT (*Tg(PCT:GAL4FF;UAS:GFP*) (Kawakami et al., 2010)). While as judged by GFP and *cdh17* mRNA expression, Kid expression in the PCT depleted cells in this segment, (Fig. S2C-E), PGC cluster length and position as well as the PGC speed remained unaffected (Fig. S2F, right graph in G), suggesting that PGCs' positioning along the anterior-posterior axis of the embryo is not dictated by the PCT.

We have previously reported on the control of dorsoventral positioning of zebrafish PGC clusters by Wunen-family proteins expressed within the developing somites (Paksa et al., 2016). The localization of PGC clusters ventral to the PCT prompted us to investigate whether it can provide an additional level of regulation to PGC positioning along this axis. Indeed, elimination of the PCT resulted in the shift of PGC clusters dorsally relative to the ventral somites' border (Fig. S2C, schematic and left graph in G).

Germ cells' motility is reduced regardless of positioning within the embryo and clustering

To determine whether PGC migration speed reduction is a response to a specific cue or to conditions at the target site, we examined the behavior of PGCs in other locations at 24-26 hpf. Here, we examined the behavior of PGCs within an ectopic cell cluster in embryos mutated for the *spadetail* gene (Weidinger et al., 1999). Interestingly, ectopic PGCs exhibited a reduction in migration speed and displacement similar to that observed for PGCs following arrival at the gonad region (Fig. 1D-H), culminating in a loss of motility by 36 hpf. Thus, these migration parameters are reduced irrespective of PGCs' location.

To investigate whether the reduction of motility observed in cell clusters is related to enhanced interactions among the cells in the cluster or to specific interactions at the target region, we examined the behavior of single cells dispersed throughout the embryo lacking the chemokine receptor Cxcr4b (Doitsidou et al., 2002) (Fig. S3A).

Interestingly, in this experiment too, we observed a reduced migration speed and displacement for single PGCs irrespective of their position (Fig. S3B-G).

Maturation of the embryonic tissue is correlated with the reduction in migration speed

To examine whether the reduction in motility reflects global stage-related changes in the tissues within which PGCs migrate, we conducted transplantation experiments. Here, we transferred PGCs between embryos of different developmental stages and monitored their migration. To validate this experimental setup we first transferred cells between embryos of the same developmental stage (Fig. 2A, B). We analyzed the migration of both donor (green) and host (magenta) PGCs and found similar migration speeds between PGCs of the host and donor embryos (Fig. 2F). We then transplanted PGCs from 35 hpf embryos ("old" PGCs) into 4.5 hpf ("young") host embryos and followed their migration (Fig. 2C-E). Interestingly, the migration speed of the "old" PGCs transplanted into the "young" embryos was higher than that of the "old" PGCs located at the gonad region (Fig. 2C-E, G).

As embryonic development progresses, the expression of ECM components in the embryo (e.g., fibronectin, collagen, etc.) increases (Gistelinck et al., 2016; Latimer and Jessen, 2010), consistent with the idea that, similar to other ameboid cell types (e.g., neutrophils, T cells, tumor cells), PGC migration could be hindered by the tissue's increasingly dense protein network (Harmansa et al., 2023; Reis-Rodrigues et al., 2025; Wolf et al., 2013). To examine this possibility, we monitored the migration speed of PGCs expressing a combination of three membrane metalloproteases (MMPs), namely MMP2, MMP9 and MMP14, which have been shown to promote cell migration (Gonzalez-Molina et al., 2019; Orgaz et al., 2014). Notably, we observed an increase in the migration speed of such PGCs, consistent with the idea that PGC migration speed slows down as the embryo develops a denser network of ECM (Fig. 2H). Similar modulation of MMP activity and, thus, ECM remodeling is crucial for immune cells to switch their migration modes (e.g., macrophages (Travnickova et al., 2021)) and for cancer cells' epithelial-to-mesenchymal transition (Brassart-Pasco et al., 2020; Yamada et al., 2019).

Together, these findings suggest that the maturation of the embryonic environment (e.g., ECM production and assembly) affects PGCs' migratory behavior.

To determine whether the environment alone can account for PGCs' decline in migration speed, we compared the behavior of "old" transplanted PGCs to that of endogenous "young" PGCs in 8 hpf host embryos (Fig. 2I). Surprisingly, while "old" PGCs migrated faster within the "young" embryo environment relative to their counterparts within "old" sibling embryos (Fig. 2G), their migration speed was lower than that of "young" host PGCs (Fig. 2I). Thus, the cessation of PGC motility at the target results from a combination of environmental effects and a PGC-intrinsic program.

Cellular events correlated with the loss of motility

Next, we examined the cellular activities, distribution of polarity marker molecules, and morphological features associated with PGC motility.

Similar to other cell types that form blebs during migration (García-Arcos et al., 2024; Georgantzoglou et al., 2022; Paluch and Raz, 2013; Robertson et al., 2025; Schick and Raz, 2022; Schick et al., 2025), zebrafish PGCs form hydrostatic pressure-powered protrusions at the cell front during their migration (Blaser et al., 2006; Goudarzi et al., 2017; Truszkowski et al., 2023). Importantly, PGCs that form a reduced number of blebs show lower motility and impaired arrival at the target region (Blaser et al., 2006; Goudarzi et al., 2017). Thus, we quantified the frequency of bleb formation of PGCs at 24-26 hpf and 34-36 hpf (Fig. 3A, B, D). To eliminate possible effects of crowding at the clustering point and to reliably evaluate blebbing activity, we analysed PGCs that were dispersed throughout the embryo (Fig. 3A). Indeed, we found that bleb frequency was significantly reduced from 24 to 36 hpf at any location within the embryo (Fig. 3B, D).

An additional process linked to the cell polarity is the accumulation of actin at the cell front, while proteins like Ezrin accumulate at the cell back (Charras and Paluch, 2008; Hoffmann et al., 2025; Olguin-Olguin et al., 2021; Truszkowski et al., 2023). Thus, we analyzed the localization and distribution of markers for the cell front (Lifeact, green in representative images Fig. 3A, quantification in C and E) and back (Ezrin, magenta in representative images Fig. 3A) in PGCs located at the gonad and ectopic positions. This analysis revealed that at 24-26 hpf, PGCs exhibited distinct

front-back polarity regardless of their location. In contrast, and in line with the loss of motility, by 34-36 hpf their polarity was lost, and Ezrin and actin were more evenly distributed within the PGCs.

Altered expression of proteins important for contractility and PGC identity

To determine the molecular basis for the reduction of blebbing activity (Fig. 3B, D) and to follow the differentiation state of the PGCs, the cells were isolated from 15, 25 and 35 hpf embryos. RNA-seq analysis was performed for PGCs at the gonad region (Fig. 3F) and for ectopically-located germ cells (in embryos lacking functional guidance receptor Cxcr4b, Fig. S4A). This analysis revealed that between 15 and 35 hpf, mRNA levels of PGC markers such as *ddx4*, *nanos3*, *tdrd7a* and *dnd1* were reduced (Figs. 3G and S4B). Similarly, transcripts encoding proteins relevant to contractility and blebbing, such as Mylk and Rock2b (Amano et al., 1996; Blaser et al., 2006; Kishi et al., 1998; Totsukawa et al., 2004), were reduced (Figs. 3H and S4C). In contrast to a decrease in mRNA levels of specification and contractility markers, we observed an increase in differentiation- and adhesion-related transcripts (e.g. Figs. 3I and S4D). Similar transcriptomic profiles were observed in PGC at the gonad region and in ectopic germ cells, consistent with the idea that PGC-intrinsic mechanisms control the loss of motility.

***dnd1* expression level controls PGC motility**

One way to explain the drop in cell motility is the dramatic decrease in the expression level of *dnd1* during the first 35 hours of embryonic development. Indeed, we and others have previously found that Dnd1 is essential for germ cell motility and fate (Goudarzi et al., 2012; Gross-Thebing et al., 2017; Mall et al., 2021; Ruthig et al., 2019; Wang et al., 2025; Weidinger et al., 2003; Westerich et al., 2023; Youngren et al., 2005). The mechanism by which Dnd1 exerts its function involves binding target RNAs, stabilizing them and enhancing their translation (Aguero et al., 2017; Kedde et al., 2007; Ruthig et al., 2023; Zhang et al., 2021). Specifically, we previously found that Dnd1 function is required for enhancing contractility and achieving actin retrograde flow, while reducing the level of adhesion (Goudarzi et al., 2012). We, therefore, hypothesized that the progressive decay of maternally

Development • Supplementary information

provided *dnd1* mRNA functions as a “molecular clock” that dictates the rate of PGC motility loss.

To test this, we examined the effect of enhanced Dnd1 level on PGC behavior upon arrival at the gonad. Here, we injected embryos with a combination of RNAs encoding for germ plasm factors, to transform all the cells in the embryo into germ cells, hereafter referred to as “induced PGCs” (iPGCs) (Wang et al., 2023). We further titrated down the amount of *dnd1* mRNA in the induction mix to the minimum sufficient to convert early blastomeres to PGCs (Dnd1-low), as determined by the successful arrival of such iPGCs at their target region by 24 hpf, as well as the expression of the PGC markers. To assess the effect of Dnd1 level on PGCs’ migratory behavior, we compared the Dnd1-low induction mix with one that included a very high level of *dnd1*-encoding RNA (Dnd1-high). iPGCs containing either of the two mixtures were transplanted into wild-type hosts lacking PGCs (Fig. 4A). We then analyzed iPGC migration and detected an increase in displacement and cell speed for iPGCs engineered to express more Dnd1 (Fig. 4B,C, Fig. S5A). We attribute the more pronounced differences in PGC displacement compared to the differences in speed to the fact that cells possessing higher contractility can better cope with obstacles in the environment without altering their migration direction as much. This allows PGCs to migrate further, which is manifested in the increase in displacement, while speed is less affected (Fig. 1, Fig. 4B,C). Furthermore, we performed transplantation experiments (Fig. 4A), employing wild-type fish as recipients (embryos with intact endogenous PGCs). The transplanted fish were subsequently reared to adulthood, and the germline transmission efficiency of the genetically labeled donor cells was assessed. Notably, germ cells engineered to express higher Dnd1 levels (Dnd1-high) demonstrated a reduction in the proportion of offspring compared to Dnd1-low counterparts (Fig. 4D, Fig. S5B). We hypothesize that the reduced germline transmission rate of Dnd1-high PGCs can be attributed to their elevated contractility and limited capacity to form functional interactions with the somatic part of the developing gonad. An additional factor that could link PGC displacement with the ability to generate gametes is the fact that the position of PGCs along the migratory route could elicit changes in pluripotency, and epigenetic reprogramming (Jaszczak et al., 2025). These findings are consistent with the idea that *dnd1*-encoding RNA constitutes a limiting factor required for germ cell migration. Accordingly, the level of maternally provided *dnd1* RNA gradually decreases, such

that by 36 hpf the protein function is minor, which results in polarity loss and a stop in migration (Fig. 4E). Interestingly, *in vitro* studies in the mouse model employing the gonad culture system have shown that germ cell motility gives rise to fractures in germline cysts, highlighting the importance of halting cell migration (Levy et al., 2024). Similar mechanisms may operate in other migratory cells when the transcription profile changes as part of differentiation, thus allowing cells to modulate motile activity as they undergo differentiation processes (e.g., myocardial precursors (Staudt and Stainier, 2012)). Analogous to our findings on the role of the RNA-binding protein Dnd1 in zebrafish, the regulation of RNA stability, localization, and translation controls a wide variety of cellular processes in other organisms. For example, the function of RNA-binding proteins that control RNA decay rates is critical for regulating signaling cascades in neurogenesis as well as for the fidelity of neuronal cell migration (La Fata et al., 2014; Messaoudi et al., 2024; Zhang et al., 2025).

Taken together, our results suggest that the combination of cell-autonomous mechanisms, especially the decay rate of *dnd1* RNA, and non-cell-autonomous mechanisms such as ECM production, can control the timing at which cell migration stops, thereby allowing cells to interact with other cell types and form a functional organ (Fig. 4E).

Materials and methods

Zebrafish maintenance

Embryos were raised at 28°C in 0.3x Danieau's solution. The embryonic developmental stages were determined according to (Kimmel et al., 1995). All the experiments and fish maintenance were performed following the regulations of the LANUV NRW. The list of transgenic and mutant animals employed in this work is presented in Table S2.

DNA constructs, mRNA synthesis and microinjection

DNA constructs used in this work are listed in Table S3. Capped sense mRNAs were synthesized using the mMessage mMachine kit (Thermo Fisher) according to

manufacturer's instructions and kept at -20°C. 2 nl of an mRNA/morpholino sample was injected at one-cell stage using glass capillaries and the PV830 Pneumatic PicoPump microinjector (WPI). Cxcr4b knockdown was achived by injection of Cxcr4b morpholino oligonucleotide (Gene Tools, 5'-AAATGATGCTATCGTAAAATTCCAT-3', 600 µM). Depletion of endogenous PGCs in transplantation experiments was achived by injection of Dnd1 morpholino oligonucleotide (Gene Tools, 5'- GCTGGGCATCCATGTCTCCGACCAT-3', 40 µM).

Microscopy and acquisition analysis

Embryos were dechorionated in 0.3x Danieau's solution (6-8 minutes at room temperature (RT)). For embryos older than 18-19 hpf, 200 mg/L of tricaine (Sigma) was added prior to imaging to inhibit movement. To prevent pigmentation, embryos after 20 hpf were transferred to 0.003% of 1-phenyl 2-thiourea (PTU) (Sigma) in 0.3x Danieau's solution. Dechorionated embryos were transferred to agarose coated (Thermo Fisher) ramps with 0.3x Danieau's solution. Dechorionated embryos older than 24 hpf were mounted laterally in 0.5% LMP agarose (Invitrogen) drops that contained 200 mg/L of tricaine (Sigma). Polymerized agarose drops were covered with 0.3x Danieau's solution that contained 200 mg/L of tricaine (Sigma). During the imaging, the embryos were maintained at 28 °C using a heating stage (PECON). The embryos were subjected to image acquisition using 10x, 20x and 40x water immersion objectives and Z-stacks were acquired from each sample on a spinning disk confocal microscope (Zeiss Imager M2, Visitron systems) using a HAMAMATSU digital camera (C13440-20CU ORCA-flash 4.0) controlled by the VisiView software (version 4.5.0.14). The Z-stacks were captured within a range of 6 - 30 µm with 2 to 4-minutes intervals (for a total of 60-120 minutes). PGC tracking, tissue drift correction, and measurements of PGC speed and displacement were performed using Imaris software (version 9.9.0). The polarity of the migrating PGCs inside and outside the gonad region was investigated by following the localized distribution of Lifeact using *Tg(kop:lifeact.mCherry)* and Ezrin using *Tg(kop:YPET.Ezrin)* fishlines at 24 to 26 hpf and at 34 to 36 hpf. 14 µm Z-stacks were acquired using a 63x water immersion objective every 2 µm with 8-seconds frame intervals. The 4D data were analyzed with the Fiji (version 2.1.0/1.53c) and Imaris software (version 9.7.2)

allowing a detailed analysis of the localized distribution of polarity markers. The blebbing frequency of the migrating PGCs inside and outside the gonad region was analyzed by farnesylated mCherry (membrane labelling) using *Tg(kop:mCherry.F')* and Lifeact distribution using *Tg(kop:EGFP-lifeact)* fishlines at 24 to 26 hpf and at 34 to 36 hpf. 14 µm Z-stacks were acquired using a 63x water-immersion objective every 2 µm with 5-seconds per frame intervals (for a total of 10 minutes). The 4D data were analyzed with the Fiji (version 2.1.0/1.53c). 5-8 minutes of the acquired data were considered for analyzing the number of blebs.

Transplantation experiments

For experiments presented in the Figure 2, donor embryos were dechorionated and treated with trypsin (Sigma) for 5 min at 31 °C followed by quick washes with dissociation buffer (Gibco). Next, the embryos were dissociated by slow pipetting with a 100 µl pipette in 50-80 µl of the cell dissociation buffer (Gibco). The dissociated cells were transferred to a glass slide and ~50 cells were immediately transplanted into host embryos. For experiments presented in the Figures 4 and S5, donor iPGCs were induced as described by Hoffmann et al., 2025 (Hoffmann et al., 2025) with addition of 400 pg of either control (Dnd1-low) or *dnd1* (Dnd1-high) mRNA. At ~ 4 hpf iPGCs from such donor embryos were transplanted into the hosts of the same age without prior dissociation. The transplantation was conducted using a stereomicroscope (Leica S8AP0) with a 50 µm transplantation needle with spike (BM100T-10, Biomedical instruments). Afterwards the embryos developed at 28 °C for 2 hours followed by microscopy. For 35 hpf *Tg(vasa:vasa-EGFP)* donor embryos, the gonad region was micro-dissected prior to dissociation. Wild-type AB or *Tg(kop:mCherry.F')* embryos at 4.3-5 hpf were employed as hosts.

PGC polarity analysis

To quantify actin signal asymmetry, mean fluorescence intensity of the Lifeact was measured at the cell boundary using a circular region of interest (ROI) with a diameter of 45 pixels. The mean intensity was measured at the brightest area of the Lifeact signal. The second measurement was taken at the opposing aspect of the

cell boundary using an ROI of identical dimensions. Asymmetry ratio was calculated by dividing the mean intensity at the brightest region by the mean intensity at the opposing region. Analysis was performed in ImageJ Version: 2.16.0/1.54p.

RNA tomography (Tomo-seq)

This method was performed as described previously in (Junker et al., 2014). In short, 24 hpf *Tg(kop:EGFP.F')* embryos were covered with Jung tissue freezing medium (Leica), oriented laterally, and the region of the developing gonad was marked by polyacrylamide beads. Next, embryos were frozen on dry ice. The labeled region (developing gonad) was sectioned into 60 sections (10 µm thickness) along the anteroposterior axis or into 48 sections (10 µm thickness) along the dorsoventral axis. Each section was transferred to pre-cooled LoBind 1.5ml tubes (Eppendorf) and kept on dry ice. RNA from each section was extracted and subjected to RNA-sequencing (for details see the corresponding Supplementary Methods section).

RNA sequencing (RNA-seq)

PGCs were sorted by fluorescence activated cell sorting (FACS), mRNA was extracted and subjected to RNA-seq (for details see the corresponding Supplementary Methods section).

Whole mount in situ hybridization and RNAscope

Preparation of the embryos and whole mount *in situ* hybridization was performed following the protocol described in (Thisse and Thisse, 2008). After staining embryos were covered with 80% glycerol (Applichem) and positioned in the correct orientation. Color images were acquired using Leica MZ16F stereomicroscope with a AxioCam MRc5 camera controlled by ZEN software (version 2012 blue edition, 1.1.1.0).

RNAscope was performed by using the RNAscope Multiplex Fluorescent Kit (Bio-techne) following the protocol described in (Gross-Thebing et al., 2014). The

embryos were mounted laterally in 1% LMP agarose drops (Invitrogen) and covered with 1x PBS. Fluorescent Z-stacks were acquired on a confocal microscope (LSM 710, Zeiss) controlled by the ZEN software (version 2010B SP1) using 20-40x water immersion objectives (Zeiss). The acquired images were processed using Fiji (version 2.1.0/1.53c) by generating maximum intensity Z-projections of the focal 42 planes containing the fluorescence signal. Brightness and contrast were adjusted similarly in both the control and treatment samples for each channel. 3D-reconstructions from fluorescent images were made in Imaris (version 9.7.2).

PGC induction

PGCs were induced as described in Hoffmann et al., 2025 (Hoffmann et al., 2025). In brief, 1-cell stage embryos were injected with the mix of 6 mRNAs (see Table S3): 100 pg *nanos3CDS.globin3'utr* (internal DB number - 278), 226 pg *vasaFL.globin3'utr* (333), 40 pg (Dnd1-low) or 400 pg (Dnd1-high) *dnd1.globin3'utr* (487), 300 pg *tdrd7.globin3'utr* (A241), 16 pg *pCS2-buc* (B639), 19 pg *tdrd6.globin3'utr* (F089) and 400 pg (Dnd1-low) or 40 pg (Dnd1-high) of stuffer mRNA. Fluorescent marker mRNA with the *nos3* 3'UTR (e.g., *mGFP.nos3'utr* (355)) was included to control for the successful PGC induction at 5-6-hpf.

Statistics

Statistical analysis was performed using Prism software (version 9). The normality of the distribution of the data was tested with D'Agostino-Pearson omnibus normality test. The significance of the data was tested with either the student's t-test (if the data were normally distributed), by Mann-Whitney U test (if the data were not normally distributed) or by Fisher's exact test. The P-values are shown on top of the graphs. If not stated otherwise, statistical analysis was performed on experiments with three independent biological replicates.

Acknowledgements

We thank Ursula Jordan, Esther-Maria Messerschmidt, and Ines Sandbote for excellent technical help. Z.L. was and L.K. is a member of CiM-IMPRS, the joint graduate school of the Cells-in-Motion Interfaculty Centre, University of Münster, Germany and the International Max Planck Research School – Molecular Biomedicine, Münster, Germany. We thank Celeste Brennecka for editing the manuscript.

Competing interests

Authors declare no competing interests

Funding

Z.L. was a fellow of the CiM-IMPRS, M.O., J.S., D.H., L.K., and E.R. are supported by funds from the University of Muenster, the Max Planck Institute for Molecular Biomedicine, the German Research Foundation (DFG) grant RA863/14-1, and the SFB 1348 project B06. J. B. K. and J. P. J are supported by the German Research Foundation (DFG) project number 540370162.

Author contribution

E.R. supervised the project; K.T., Z. L. and E.R. designed the work and wrote the manuscript; K.T. and Z. L. performed all experiments except for the following: D. H. performed imaging and analysis of the PGC migration in control and PCT-ablated embryos (Fig. S2G, right graph), S. G-T. analysed PGC blebbing (Fig. 3B, D), L. K. performed statistical analysis on the data presented in the Fig. 4D and Fig. S5B (raw data acquired by K. T.), J. S. analysed PGC polarity (Fig. 3C, E) and designed graph Fig. S5A (raw data acquired by K. T.), M. S. performed FACS, Jo. S. and C. R. conducted RNA-sequencing and preliminary analysis of the data. M. R-F., M. O., Z. L., J. B. K. and J. P. J performed RNA tomography experiments. Z. L. and M. O. carried out candidate screening based on the RNA tomography data. All authors read and approved the final manuscript with minor revisions.

Data and resource availability

Source data and plasmids generated in this study are available from the lead contact (erez.raz@uni-muenster.de). Raw data of the RNA-seq experiments presented in the manuscript are available on GEO: GSE310575 (bulk mRNA sequencing) and GSE313050 (RNA tomography).

References

Aguero, T., Jin, Z., Chorghade, S., Kalsotra, A., King, M. L. and Yang, J. (2017). Maternal Dead-end 1 promotes translation of *nanos1* by binding the eIF3 complex. *Development* **144**, 3755–3765.

Amano, M., Ito, M., Kimura, K., Fukata, Y., Chihara, K., Nakano, T., Matsuura, Y. and Kaibuchi, K. (1996). Phosphorylation and Activation of Myosin by Rho-associated Kinase (Rho-kinase). *Journal of Biological Chemistry* **271**, 20246–20249.

Ara, T., Tokoyoda, K., Sugiyama, T., Egawa, T., Kawabata, K. and Nagasawa, T. (2003). Long-Term Hematopoietic Stem Cells Require Stromal Cell-Derived Factor-1 for Colonizing Bone Marrow during Ontogeny. *Immunity* **19**, 257–267.

Blaser, H., Reichman-Fried, M., Castanon, I., Dumstrei, K., Marlow, F. L., Kawakami, K., Solnica-Krezel, L., Heisenberg, C.-P. and Raz, E. (2006). Migration of Zebrafish Primordial Germ Cells: A Role for Myosin Contraction and Cytoplasmic Flow. *Developmental Cell* **11**, 613–627.

Brassart-Pasco, S., Brézillon, S., Brassart, B., Ramont, L., Oudart, J.-B. and Monboisse, J. C. (2020). Tumor Microenvironment: Extracellular Matrix Alterations Influence Tumor Progression. *Front. Oncol.* **10**,.

Charras, G. and Paluch, E. (2008). Blebs lead the way: how to migrate without lamellipodia. *Nat Rev Mol Cell Biol* **9**, 730–736.

Coombs, C., Georgantzoglou, A., Walker, H. A., Patt, J., Merten, N., Poplimont, H., Busch-Nentwich, E. M., Williams, S., Kotsi, C., Kostenis, E., et al. (2019). Chemokine receptor trafficking coordinates neutrophil clustering and dispersal at wounds in zebrafish. *Nat Commun* **10**, 5166.

Cortés, F., Daggett, D., Bryson-Richardson, R. J., Neyt, C., Maule, J., Gautier, P., Hollway, G. E., Keenan, D. and Currie, P. D. (2003). Cadherin-Mediated Differential Cell Adhesion Controls Slow Muscle Cell Migration in the Developing Zebrafish Myotome. *Developmental Cell* **5**, 865–876.

Doitsidou, M., Reichman-Fried, M., Stebler, J., Köprunner, M., Dörries, J., Meyer, D., Esguerra, C. V., Leung, T. and Raz, E. (2002). Guidance of Primordial Germ Cell Migration by the Chemokine SDF-1. *Cell* **111**, 647–659.

Doren, M. V. and Lehmann, R. (1997). Cell migration: Don't tread on me. *Current Biology* **7**, R148–R150.

García-Arcos, J. M., Jha, A., Waterman, C. M. and Piel, M. (2024). Blebology: principles of bleb-based migration. *Trends in Cell Biology* **34**, 838–853.

Georgantzoglou, A., Poplimont, H., Walker, H. A., Lämmermann, T. and Sarris, M. (2022). A two-step search and run response to gradients shapes leukocyte navigation in vivo. *Journal of Cell Biology* **221**, e202103207.

Gistelinck, C., Gioia, R., Gagliardi, A., Tonelli, F., Marchese, L., Bianchi, L., Landi, C., Bini, L., Huysseune, A., Witten, P. E., et al. (2016). Zebrafish Collagen Type I: Molecular and Biochemical Characterization of the Major Structural Protein in Bone and Skin. *Sci Rep* **6**,.

Gonzalez-Molina, J., Gramolelli, S., Liao, Z., Carlson, J. W., Ojala, P. M. and Lehti, K. (2019). MMP14 in Sarcoma: A Regulator of Tumor Microenvironment Communication in Connective Tissues. *Cells* **8**, 991.

Goudarzi, M., Banisch, T. U., Mobin, M. B., Maghelli, N., Tarbashevich, K., Strate, I., van den Berg, J., Blaser, H., Bandemer, S., Paluch, E., et al. (2012). Identification and Regulation of a Molecular Module for Bleb-Based Cell Motility. *Developmental Cell* **23**, 210–218.

Goudarzi, M., Tarbashevich, K., Mildner, K., Begemann, I., Garcia, J., Paksa, A., Reichman-Fried, M., Mahabaleshwar, H., Blaser, H., Hartwig, J., et al. (2017). Bleb Expansion in Migrating Cells Depends on Supply of Membrane from Cell Surface Invaginations. *Developmental Cell* **43**, 577-587.e5.

Grimaldi, C. and Raz, E. (2020). Germ cell migration—Evolutionary issues and current understanding. *Seminars in Cell & Developmental Biology* **100**, 152–159.

Gross-Thebing, T., Paksa, A. and Raz, E. (2014). Simultaneous high-resolution detection of multiple transcripts combined with localization of proteins in whole-mount embryos. *BMC Biol* **12**, 55.

Gross-Thebing, T., Yigit, S., Pfeiffer, J., Reichman-Fried, M., Bandemer, J., Ruckert, C., Rathmer, C., Goudarzi, M., Stehling, M., Tarbashevich, K., et al. (2017). The Vertebrate Protein Dead End Maintains Primordial Germ Cell Fate by Inhibiting Somatic Differentiation. *Developmental Cell* **43**, 704-715.e5.

Harmansa, S., Erlich, A., Eloy, C., Zurlo, G. and Lecuit, T. (2023). Growth anisotropy of the extracellular matrix shapes a developing organ. *Nat Commun* **14**, 1220.

Herpin, A., Fischer, P., Liedtke, D., Kluever, N., Neuner, C., Raz, E. and Schartl, M. (2008). Sequential SDF1a and b-induced mobility guides Medaka PGC migration. *Developmental Biology* **320**, 319–327.

Hoffmann, D., Agranov, T., Kühl, L., Ermlich, L., Reichman-Fried, M., Simons, B. D., Gov, N. S. and Raz, E. (2025). Corrections in single-cell migration path in vivo are controlled by pulses in polar Rac1 activation. *Current Biology* **35**, 4365-4382.e8.

Jaszczak, R. G., Zussman, J. W., Wagner, D. E. and Laird, D. J. (2025). Comprehensive profiling of migratory primordial germ cells reveals niche-specific differences in non-canonical Wnt and Nodal-Lefty signaling in anterior vs posterior migrants.

Junker, J. P., Noël, E. S., Guryev, V., Peterson, K. A., Shah, G., Huisken, J., McMahon, A. P., Berezikov, E., Bakkers, J. and van Oudenaarden, A. (2014). Genome-wide RNA Tomography in the Zebrafish Embryo. *Cell* **159**, 662–675.

Kawakami, K., Abe, G., Asada, T., Asakawa, K., Fukuda, R., Ito, A., Lal, P., Mouri, N., Muto, A., Suster, M. L., et al. (2010). zTrap: zebrafish gene trap and enhancer trap database. *BMC Dev Biol* **10**, 105.

Kedde, M., Strasser, M. J., Boldajipour, B., Vrielink, J. A. F. O., Slanchev, K., Le Sage, C., Nagel, R., Voorhoeve, P. M., Van Duijse, J., Ørom, U. A., et al. (2007). RNA-Binding Protein Dnd1 Inhibits MicroRNA Access to Target mRNA. *Cell* **131**, 1273–1286.

Kienle, K., Glaser, K. M., Eickhoff, S., Mihlan, M., Knöpper, K., Reátegui, E., Epple, M. W., Gunzer, M., Baumeister, R., Tarrant, T. K., et al. (2021). Neutrophils self-limit swarming to contain bacterial growth in vivo. *Science* **372**, eabe7729.

Kimmel, C. B., Ballard, W. W., Kimmel, S. R., Ullmann, B. and Schilling, T. F. (1995). Stages of embryonic development of the zebrafish. *Developmental Dynamics* **203**, 253–310.

Kishi, H., Ye, L.-H., Nakamura, A., Okagaki, T., Iwata, A., Tanaka, T. and Kohama, K. (1998). Structure and Function of Smooth Muscle Myosin Light Chain Kinase. In *Mechanisms of Work Production and Work Absorption in Muscle* (ed. Sugi, H.) and Pollack, G. H.), pp. 229–234. Boston, MA: Springer US.

Knaut, H., Werz, C., Geisler, R., Nüsslein-Volhard, C. and Tübingen 2000 Screen Consortium (2003). A zebrafish homologue of the chemokine receptor Cxcr4 is a germ-cell guidance receptor. *Nature* **421**, 279–282.

Köprunner, M., Thisse, C., Thisse, B. and Raz, E. (2001). A zebrafish *nanos* -related gene is essential for the development of primordial germ cells. *Genes Dev.* **15**, 2877–2885.

La Fata, G., Gärtner, A., Domínguez-Iturza, N., Dresselaers, T., Dawitz, J., Poorthuis, R. B., Averna, M., Himmelreich, U., Meredith, R. M., Achsel, T., et al. (2014). FMRP regulates multipolar to bipolar transition affecting neuronal migration and cortical circuitry. *Nat Neurosci* **17**, 1693–1700.

Labbaf, Z., Petratou, K., Ermlich, L., Backer, W., Tarbashevich, K., Reichman-Fried, M., Luschnig, S., Schulte-Merker, S. and Raz, E. (2022). A robust and tunable system for targeted cell ablation in developing embryos. *Developmental Cell* **57**, 2026-2040.e5.

Latimer, A. and Jessen, J. R. (2010). Extracellular matrix assembly and organization during zebrafish gastrulation. *Matrix Biology* **29**, 89–96.

Mall, E. M., Lecanda, A., Drexler, H. C. A., Raz, E., Schöler, H. R. and Schlatt, S. (2021). Heading towards a dead end: The role of DND1 in germ line differentiation of human iPSCs. *PLoS ONE* **16**, e0258427.

Messaoudi, S., Allam, A., Stoufflet, J., Paillard, T., Le Ven, A., Fouquet, C., Doulazmi, M., Trembleau, A. and Caille, I. (2024). FMRP regulates postnatal neuronal migration via MAP1B. *eLife* **12**, RP88782.

Minina, S., Reichman-Fried, M. and Raz, E. (2007). Control of Receptor Internalization, Signaling Level, and Precise Arrival at the Target in Guided Cell Migration. *Current Biology* **17**, 1164–1172.

Miskolci, V., Klemm, L. C. and Huttenlocher, A. (2021). Cell Migration Guided by Cell–Cell Contacts in Innate Immunity. *Trends in Cell Biology* **31**, 86–94.

Molon, B., Liboni, C. and Viola, A. (2022). CD28 and chemokine receptors: Signalling amplifiers at the immunological synapse. *Front. Immunol.* **13**, 938004.

Molyneaux, K. A., Zinszner, H., Kunwar, P. S., Schaible, K., Stebler, J., Sunshine, M. J., O'Brien, W., Raz, E., Littman, D., Wylie, C., et al. (2003). The chemokine SDF1/CXCL12 and its receptor CXCR4 regulate mouse germ cell migration and survival. *Development* **130**, 4279–4286.

Nishiumi, F., Komiya, T. and Ikenishi, K. (2005). The mode and molecular mechanisms of the migration of presumptive PGC in the endoderm cell mass of *Xenopus* embryos. *Dev Growth Differ* **47**, 37–48.

Olguin-Olguin, A., Aalto, A., Maugis, B., Boquet-Pujadas, A., Hoffmann, D., Ermlich, L., Betz, T., Gov, N. S., Reichman-Fried, M. and Raz, E. (2021). Chemokine-biased robust self-organizing polarization of migrating cells in vivo. *Proc. Natl. Acad. Sci. U.S.A.* **118**, e2018480118.

Orgaz, J. L., Pandya, P., Dalmeida, R., Karagiannis, P., Sanchez-Laorden, B., Viros, A., Albrengues, J., Nestle, F. O., Ridley, A. J., Gaggioli, C., et al. (2014). Diverse matrix metalloproteinase functions regulate cancer amoeboid migration. *Nat Commun* **5**, 4255.

Paksa, A., Bandemer, J., Hoeckendorf, B., Razin, N., Tarbashevich, K., Minina, S., Meyen, D., Biundo, A., Leidel, S. A., Peyrieras, N., et al. (2016). Repulsive cues combined with physical barriers and cell–cell adhesion determine progenitor cell positioning during organogenesis. *Nat Commun* **7**, 11288.

Paluch, E. K. and Raz, E. (2013). The role and regulation of blebs in cell migration. *Current Opinion in Cell Biology* **25**, 582–590.

Reichman-Fried, M., Minina, S. and Raz, E. (2004). Autonomous Modes of Behavior in Primordial Germ Cell Migration. *Developmental Cell* **6**, 589–596.

Reis-Rodrigues, P., Avellaneda, M. J., Canigova, N., Gaertner, F., Vaahtomeri, K., Riedl, M., De Vries, I., Merrin, J., Hauschild, R., Fukui, Y., et al. (2025). Migrating immune cells globally coordinate protrusive forces. *Nat Immunol* **26**, 1258–1266.

Robertson, T. F., Schrope, J., Zwick, Z., Rindy, J., Horn, A., Hou, Y. and Huttenlocher, A. (2025). Live imaging in zebrafish reveals tissue-specific strategies for amoeboid migration. *Development* **152**, dev204351.

Roycroft, A. and Mayor, R. (2016). Molecular basis of contact inhibition of locomotion. *Cell. Mol. Life Sci.* **73**, 1119–1130.

Ruthig, V. A., Friedersdorf, M. B., Garness, J. A., Munger, S. C., Bunce, C., Keene, J. D. and Capel, B. (2019). The RNA-binding protein DND1 acts sequentially as a negative regulator of pluripotency and a positive regulator of epigenetic modifiers required for germ cell reprogramming. *Development* **146**, dev175950.

Ruthig, V. A., Hatkevich, T., Hardy, J., Friedersdorf, M. B., Mayère, C., Nef, S., Keene, J. D. and Capel, B. (2023). The RNA binding protein DND1 is elevated in a subpopulation of pro-spermatogonia and targets chromatin modifiers and translational machinery during late gestation. *PLoS Genet* **19**, e1010656.

Schick, J. and Raz, E. (2022). Blebs—Formation, Regulation, Positioning, and Role in Amoeboid Cell Migration. *Front. Cell Dev. Biol.* **10**, 926394.

Schick, J., Ermlich, L., Kühl, L., Hoffmann, D. and Raz, E. (2025). Single-cell migration in development – Lessons from germ cells. In *Current Topics in Developmental Biology*, p. S0070215325000134. Elsevier.

Shellard, A. and Mayor, R. (2019). Integrating chemical and mechanical signals in neural crest cell migration. *Current Opinion in Genetics & Development* **57**, 16–24.

Staudt, D. and Stainier, D. (2012). Uncovering the Molecular and Cellular Mechanisms of Heart Development Using the Zebrafish. *Annu. Rev. Genet.* **46**, 397–418.

Stebler, J., Spieler, D., Slanchev, K., Molyneaux, K. A., Richter, U., Cojocaru, V., Tarabykin, V., Wylie, C., Kessel, M. and Raz, E. (2004). Primordial germ cell migration in the chick and mouse embryo: the role of the chemokine SDF-1/CXCL12. *Developmental Biology* **272**, 351–361.

Takeuchi, T., Tanigawa, Y., Minamide, R., Ikenishi, K. and Komiya, T. (2010). Analysis of SDF-1/CXCR4 signaling in primordial germ cell migration and survival or differentiation in Xenopus laevis. *Mechanisms of Development* **127**, 146–158.

Tarbashevich, K., Reichman-Fried, M., Grimaldi, C. and Raz, E. (2015). Chemokine-Dependent pH Elevation at the Cell Front Sustains Polarity in Directionally Migrating Zebrafish Germ Cells. *Current Biology* **25**, 1096–1103.

Thisse, C. and Thisse, B. (2008). High-resolution in situ hybridization to whole-mount zebrafish embryos. *Nat Protoc* **3**, 59–69.

Totsukawa, G., Wu, Y., Sasaki, Y., Hartshorne, D. J., Yamakita, Y., Yamashiro, S. and Matsumura, F. (2004). Distinct roles of MLCK and ROCK in the regulation of membrane protrusions and focal adhesion dynamics during cell migration of fibroblasts. *The Journal of Cell Biology* **164**, 427–439.

Travnickova, J., Nhim, S., Abdellaoui, N., Djouad, F., Nguyen-Chi, M., Parmeggiani, A. and Kissa, K. (2021). Macrophage morphological plasticity and migration is Rac signalling and MMP9 dependant. *Sci Rep* **11**,.

Truszkowski, L., Batur, D., Long, H., Tarbashevich, K., Vos, B. E., Trappmann, B. and Raz, E. (2023). Primordial germ cells adjust their protrusion type while migrating in different tissue contexts *in vivo*. *Development* **150**, dev200603.

Wang, H., Teng, Y., Xie, Y., Wang, B., Leng, Y., Shu, H. and Deng, F. (2013). Characterization of the carbonic anhydrases 15b expressed in PGCs during early zebrafish development. *Theriogenology* **79**, 443–452.

Wang, X., Zhu, J., Wang, H., Deng, W., Jiao, S., Wang, Y., He, M., Zhang, F., Liu, T., Hao, Y., et al. (2023). Induced formation of primordial germ cells from zebrafish blastomeres by germplasm factors. *Nat Commun* **14**, 7918.

Wang, Z., Yu, H., Gu, Z., Shi, X., Ma, J., Shao, Q., Yao, Y., Yao, S., Xu, Y., Gu, Y., et al. (2025). RNA-binding proteins DND1 and NANOS3 cooperatively suppress the entry of germ cell lineage. *Nat Commun* **16**, 4792.

Weidinger, G., Wolke, U., Köprunner, M., Klinger, M. and Raz, E. (1999). Identification of tissues and patterning events required for distinct steps in early migration of zebrafish primordial germ cells. *Development* **126**, 5295–5307.

Weidinger, G., Stebler, J., Slanchev, K., Dumstrei, K., Wise, C., Lovell-Badge, R., Thisse, C., Thisse, B. and Raz, E. (2003). dead end, a Novel Vertebrate Germ Plasm Component, Is Required for Zebrafish Primordial Germ Cell Migration and Survival. *Current Biology* **13**, 1429–1434.

Westerich, K. J., Tarbashevich, K., Schick, J., Gupta, A., Zhu, M., Hull, K., Romo, D., Zeuschner, D., Goudarzi, M., Gross-Thebing, T., et al. (2023). Spatial organization and function of RNA molecules within phase-separated condensates in zebrafish are controlled by Dnd1. *Developmental Cell* **58**, 1578-1592.e5.

Wingert, R. A. and Davidson, A. J. (2008). The zebrafish pronephros: A model to study nephron segmentation. *Kidney International* **73**, 1120–1127.

Wolf, K., Te Lindert, M., Krause, M., Alexander, S., Te Riet, J., Willis, A. L., Hoffman, R. M., Figdor, C. G., Weiss, S. J. and Friedl, P. (2013). Physical limits of cell migration: Control by ECM space and nuclear deformation and tuning by proteolysis and traction force. *Journal of Cell Biology* **201**, 1069–1084.

Yamada, K. M., Collins, J. W., Cruz Walma, D. A., Doyle, A. D., Morales, S. G., Lu, J., Matsumoto, K., Nazari, S. S., Sekiguchi, R., Shinsato, Y., et al. (2019). Extracellular matrix dynamics in cell migration, invasion and tissue morphogenesis. *Int J Experimental Path* **100**, 144–152.

Yamaguchi, N. and Knaut, H. (2022). Focal adhesion-mediated cell anchoring and migration: from *in vitro* to *in vivo*. *Development* **149**, dev200647.

Youngren, K. K., Coveney, D., Peng, X., Bhattacharya, C., Schmidt, L. S., Nickerson, M. L., Lamb, B. T., Deng, J. M., Behringer, R. R., Capel, B., et al. (2005). The Ter mutation in the dead end gene causes germ cell loss and testicular germ cell tumours. *Nature* **435**, 360–364.

Zhang, Y., Godavarthi, J. D., Williams-Villalobo, A., Polk, S. and Matin, A. (2021). The Role of DND1 in Cancers. *Cancers* **13**, 3679.

Zhang, F., Fu, Y., Jimenez-Cyrus, D., Zhao, T., Shen, Y., Sun, Y., Zhang, Z., Wang, Q., Kawaguchi, R., Geschwind, D. H., et al. (2025). m6A/YTHDF2-mediated mRNA decay targets TGF-β signaling to suppress the quiescence acquisition of early postnatal mouse hippocampal NSCs. *Cell Stem Cell* **32**, 144-156.e8.

Development • Supplementary information

Figures

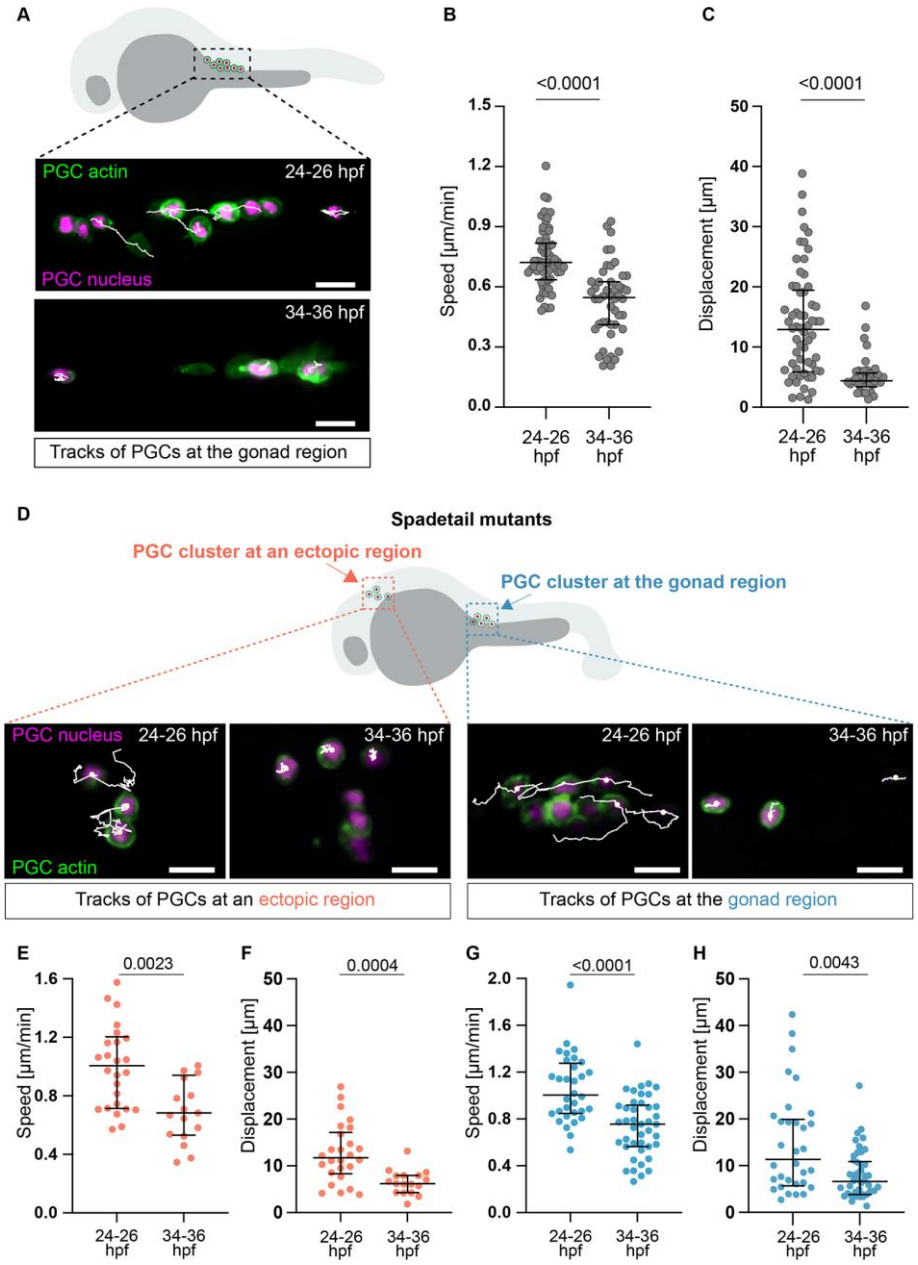

Fig. 1. Reduction in PGC migration speed during development. A. PGCs at the gonad region at 24 - 36hpf. **B-C.** PGC speed (**B**) and displacement (**C**) over 60 min. 24-26 hpf: 8 embryos, 60 PGCs; 34-36 hpf: 12 embryos, 48 PGCs. **D.** PGC clusters at the gonad and the head at 24 - 36hpf. **E-F.** PGC speed (**E**) and displacement (**F**) in ectopic clusters over 60 min. 24-26 hpf: 11 embryos, 26 PGCs; 34-36 hpf: 10 embryos, 17 PGCs. **G-H.** PGC speed (**G**) and displacement (**H**) at the gonad over 60 min. 24-26 hpf: 12 embryos, 32 PGCs; 34-36 hpf: 11 embryos, 42 PGCs. T-test, error bars: IQR. Scale bar: 20 µm.

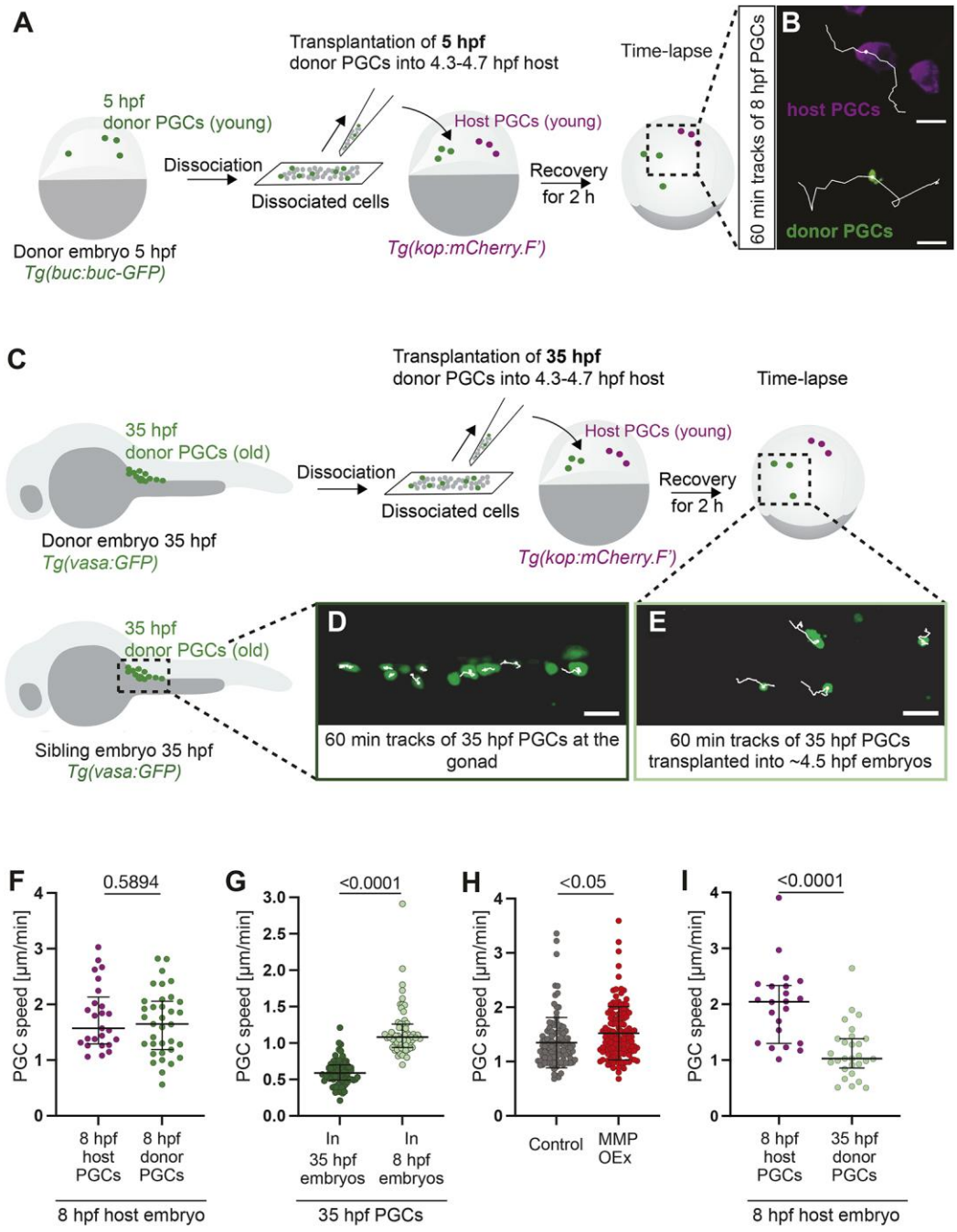

Fig. 2. PGC migration speed is controlled by environmental cues and a cell-intrinsic program. A. 5 hpf embryos were dissociated, and the mixture of labeled PGCs (green) and somatic cells (gray) was transferred into wild-type embryos. **B.** Tracks of “young” donor PGCs and “young” host PGCs within “young” host (7-9 hpf). Scale bar: 20 µm. **C.** Gonad regions of 35 hpf embryos were dissociated. This mixture of labeled PGCs (green) and somatic cells (gray) was transferred into wild-type embryos **D-E.** Tracks of “old” PGCs in control embryos (no transplantation) at 35 hpf (**D**) and of “old” donor PGCs transplanted into “young” host (**E**). Scale bar: 30

µm. **F.** Speed of “young” host and donor cells within “young” hosts (see **B**). 12 embryos with 25 PGCs (host); 20 embryos with 35 PGCs (donor). **G.** Speed of 35 hpf (“old’) PGCs at the gonad of control sibling embryos (“old”) (see **D**) and within “young” host embryos (see **E**). 19 embryos and 75 PGCs (35 hpf gonad), 14 embryos and 63 PGCs (35 hpf transplanted). **H.** Speed of PGCs overexpressing MMPs, relative to control at 24-26 hpf. Control: 36 embryos, 110 PGCs; MMP overexpression: 36 embryos, n = 131 cells. **I**. Speed of “young” host (8 hpf) and “old” donor (35 hpf) PGCs in “young” host embryos (see C and **E**). 12 embryos, 22 PGCs (host); 28 PGCs (donor). T-test, error bars: IQR.

Development • Supplementary information

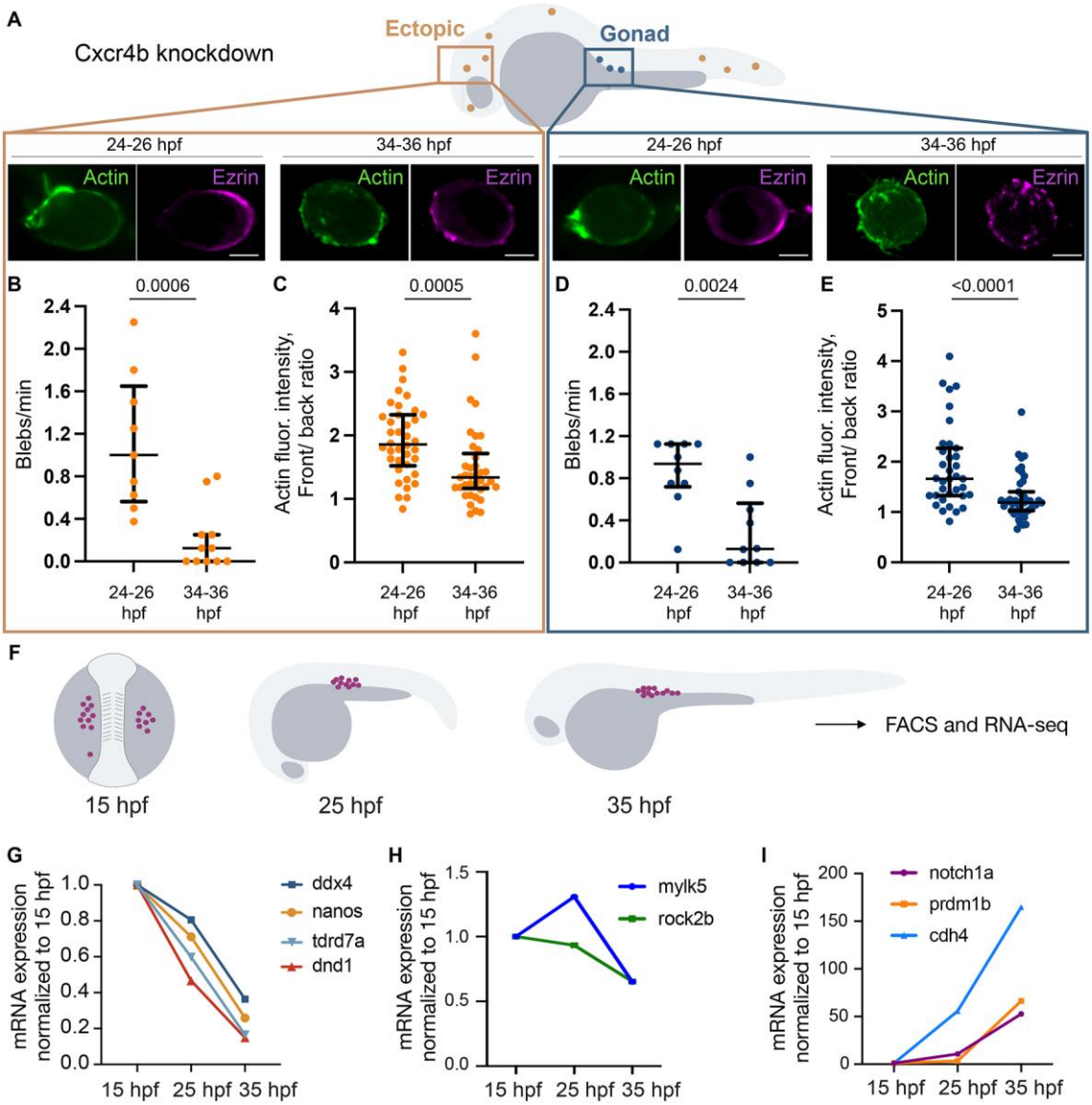

Fig. 3. Cellular events during motility loss. A. PGCs at gonad region and ectopic positions were examined for blebing activity and polarity. Localization of Lifeact and Ezrin in ectopic and gonadal PGCs. Scale bar: 5 µm. **B** and **D.** Blebing frequency in ectopic PGCs (**B**) and in PGCs at the gonad (**D**). Ectopic PGCs: 9 (24-26 hpf), 11 (34-36 hpf); gonadal PGCs: 10 (24-26 hpf), 10 (34-36 hpf). **C** and **E**. Quantification of the PGC polarity based on the cell front/ back ratio for the Lifeact fluorescence. Ectopic PGCs: 38 (24-26 hpf), 37 (34-36 hpf); gonadal PGCs: 35 (24-26 hpf), 43 (34-36 hpf). **B-E**. Mann-Whitney test, error bars: IQR. **F.** 15-35 hpf embryos were used for FACS of PGCs (magenta) and sequencing. **G-I.** Normalized levels of mRNAs important for PGC development (**G**), contractility (**H),** adhesion/differentiation (**I**).

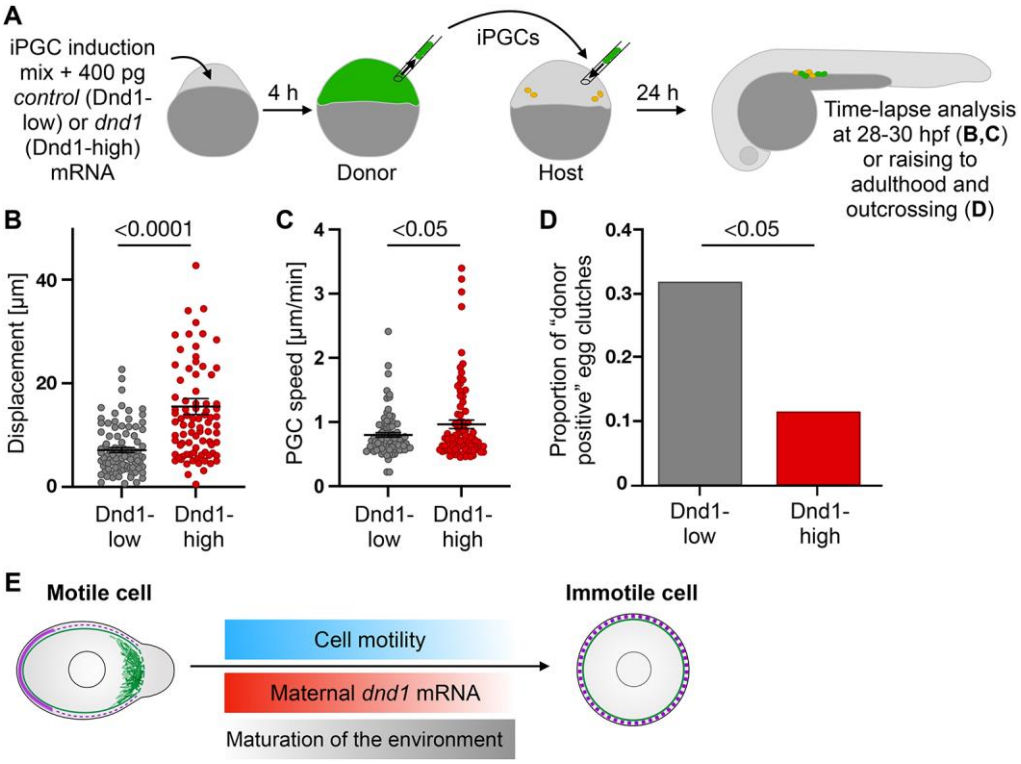

Fig. 4. *Control of motility loss by dnd1*. A. iPGCs were transplanted either into PGC-depleted (experiments presented in **B**-**C**) or into wild-type (experiment presented in **D** and **Fig. S5B**) hosts. At 28 hpf transplanted iPGCs were identified by the fluorescent marker (green). Endogenous PGCs in wild-type hosts are marked in orange. (**B-C**) iPGC displacement (**B**) and speed (**C**). T-test, error bars: SEM. 91 (Dnd1-low) and 83 (Dnd1-high) PGCs. **D.** iPGCs were transplanted into wild-type embryos that were raised and outcrossed. Fish were considered positive if they produced fluorescently labelled embryos. P = 0.033, odds ratio = 3.62 (Fisher's exact test), 41 (Dnd1-low) and 44 (Dnd1-high) animals. Error bars: CI 95%. **E.** Motile PGCs (left) express high levels of Dnd1, and are polarized (actin in green at the cell front, and back markers at the rear (magenta)). Later, *dnd1* level declines (red gradient), motility is reduced (blue gradient), while tissue rigidity (e.g., ECM level) and adhesion rise (grey gradient) culminating in stop of migration.

Development • Supplementary information

Supplementary Methods

RNA tomography (Tomo-seq)

RNA from each section was extracted using 0.5 ml TRIzol reagent (Thermo Fisher) (at RT) mixed with 0.5 µl GlycoBlue (Ambion) and 1 µl of ERCC of spike-in (Ambion) diluted 1:50,000. After 15 seconds of vigorous shaking and 5 minutes of incubation at RT, 100 µl of chloroform was added to each sample and followed by 15 seconds of vigorous shaking and 5 minutes of incubation at RT and centrifugation at 12,000 g for 15 minutes at 4°C. The aqueous supernatant was transferred to LoBind 1.5 ml tubes (Eppendorf) with 250 µl isopropanol and were vigorously shaken for 15 seconds and incubated at -20°C for 1 h to ON. Next, the samples were spun down at 12,000 g for 10 minutes at 4°C. The supernatant was removed, and the pellet was washed with 75% ethanol (7,500 g for 5 minutes at 4 °C). At last, the pellet was air dried at RT. This step was followed by reverse transcription and *in vitro* transcription with the MessageAmpII kit (Ambion) following the CEL-seq method with minor modifications as described previously (Hashimshony et al., 2012) and following the instructions of the MessageAmpII kit. The first step was first strand synthesis using barcoded primers (5 ng/µl). To each sample one barcoded primer was added. This was followed by the second strand synthesis and cDNA clean-up. Prior to cDNA clean-up all the samples were pooled together. Next, cDNA amplification was performed by *in vitro* transcription of the cDNA. Afterwards, 5.5 µl RNA fragmentation buffer per sample was added, and the samples were incubated at 94°C for 3-6 minutes. The reaction was stopped by quickly transferring the samples on ice and addition of 2.75 µl of 0.5 M EDTA. The samples were then cleaned up using 1.8x Agencourt RNAClean XP beads. The concentration of the amplified RNA was measured using the Qubit RNA high sensitivity kit (Thermo Fisher) and RNA size distribution was assessed by an RNA High Sensitivity ScreenTape assay using a TapeStation system (Agilent). The RNA was diluted to a maximum of 50 ng/µL in a volume of 5 µL for the second reverse transcription (RT). 0.5 µL of the second RT primer (random hexamers, 250 ng/µL) and 0.5 µL dNTPs (10 mM total) were added to the RNA and incubated for 5 min at 65 °C, then immediately cooled on ice. Subsequently, first strand buffer (5X, Thermo Fisher), 1 µL DTT (0,1 M), 0.5 µL RNase Out and 0.5 µL SuperScript II reverse transcriptase

Development • Supplementary information

(Thermo Fisher) were added and the cDNA was generated. In a final PCR, the second Illumina sequencing adaptor and the respective indices were introduced. The resulting cDNA libraries was purified twice using Agencourt AMPure XP beads (Beckman Coulter). The DNA concentration and size distribution of the purified libraries were measured using the Qubit DNA high sensitivity assay kit and a D1000 ScreenTape® on an Agilent TapeStation system. The fragment distribution peaked at 200-500 bp. Two libraries for each sectioning direction were sequenced paired-end on an Illumina NextSeq500 using 75% of a High-Output flow cell. Read lengths were set to 70 for the first read (R1), containing the section barcoded and unique molecular identifier and 80 for the second read (R2) that is mapped to the transcriptome. Reads were aligned with STAR (Dobin et al., 2013) using STARsolo in droplet mode. Read counts of each gene were normalized to total counts per section. To find genes with a similar expression pattern to PGCs, *vasa (ddx4)* (PGC specific gene) was used as a reference gene and all the other genes were ranked based on their similarity to *vasa* expression pattern in 2D. The ranking was performed by calculating the Euclidean distance of Z-score transformed read counts of each gene in each section to *vasa.* Since tomo-seq was performed in two orientations (along the AP and DV axis), these data were combined by averaging the Euclidean distances and the read counts.

RNA sequencing (RNA-seq)

PGCs were sorted by fluorescence activated cell sorting (FACS) technique using a FACSAria IIIu cell sorter (BD Bioscience) equipped with a 70 µm nozzle at 15, 25 and 35 hpf into the lysis buffer. *Tg(kop:mCherry.F')* and *ody;Tg(kop:mCherry.F')* fishlines were used. Embryos at 15 and 25 hpf were collected and dechorionated by using 5 mg/ml protease (Sigma) while shaking for 6-8 minutes at RT. Next 100 embryos were collected in 2 ml tubes (Eppendorf) and incubated with 1 ml trypsin for 5-8 minutes at 31 °C. Trypsin was removed and the embryos were washed 2x with 500 µl (5 µl per embryo) of cell dissociation buffer (enzyme free, PBS based, Gibco). Afterwards, the embryos were dissociated in 400-500 µl of the cell dissociation buffer (Gibco) by gently pipetting up and down with a glass pipette (50-60 times). Next, the cell dissociation mixture was filtered through a 50 µm filter (Filtrix, 50 µm, Cytecs) and kept on ice until sorting. At 35 hpf, following dechorionation using 5 mg/ml protease (Sigma) (analogous to 15 and 25 hpf embryos) 100-120 embryos were collected in 2 ml tube

Development • Supplementary information

(Eppendorf) and were incubated with 1 ml of trypsin at 31 °C for 25 minutes. Next, embryos were disintegrated by slowly pipetting 40-60 times with a glass Pasteur pipette (Brand). The dissociated embryos were then filtered through a 50 µm filter (Filtrix, 50 µm, Cytecs) and were kept on ice. The flow through was then spun down at 400 g for 5 min (RT). Supernatant was removed and the pellet was resuspended in 400 - 500 µl of the cell dissociation buffer (Gibco) by pipetting for 10-20 times with a glass Pasteur pipette (Brand). This mixture was loaded on a 30 µm filter (Filtrix, 30 µm, Cytecs) into a 1.5 ml tube (Eppendorf) which was already cooled on ice. The filter was rinsed with 100 µl of the cell dissociation buffer (Gibco). The sample was kept on ice until cell sorting. The number of cells used for 15 hpf varied from 10000 - 13000, for 25 hpf from 8000 - 12000, and for 35 hpf from 6000 - 9000.

Total RNA was extracted using the PicoPure RNA extraction kit (Arcturus) following the manufacturer's instructions. The RNA was eluted in 30 µl of elution buffer (provided by the kit) and then purified using DNA-free kit (Thermo Fisher) 38 following the protocol provided by the manufacturer. 3 µl was used for checking the quality and concentration of the RNA and the rest was used for cDNA library preparation. The RNA was stored at -20 °C. mRNA was extracted from the total RNA using NEXTflex Poly(A) Beads (Hiss Diagnostics) following the manufacturer's instructions. 14 µl of the mRNA elute was transferred to a fresh 1.5 ml tube (Eppendorf). Next, cDNA was synthesized using the NEXTflex Rapid directional qRNA-Seq kit (Hiss Diagnostics) in six steps: RNA fragmentation, first strand synthesis, second strand synthesis, adenylation, adapter ligation, and PCR amplification. All the steps followed the manufacturer's protocol. After steps 3, 5 and 6 the solution was cleaned up using AMPure XP Magnetic Beads (Beckman Coulter) and following the manufacturer's protocol. In the last clean up step, the beads were rehydrated and resuspended in 14 µl of the resuspension buffer (included in the kit) followed by 2-minute incubation at RT and 5 min incubation on a magnetic stand until the supernatant was clear. 13 µl of the clear supernatant was transferred to a 1.5 ml tube (Eppendorf) and stored at -20 °C. 3 µl was used for determining the concentration and the quality of the cDNA library and the rest was used in the following steps. The Next-generation RNA-sequencing (RNA-seq) was performed on an Illumina NextSeq 550 machine using 2x 75 bp paired-end reads. To quantify transcripts from raw fastq files Salmon mapping-based mode (Patro et al., 2017) was used. Transcript information from Ensembl (Cunningham et al., 2019)

Development • Supplementary information

release 97 for Danio_rerio GRCz11 was utilized. Genes with less than ten reads in all samples were filtered out. Gene-level differential expression between groups was assessed by calculating the log2 of the fold change of the relevant stages. The threshold was set based on expression of PGC enriched genes such as *sod2* (Tarbashevich et al., 2023).

Development • Supplementary information

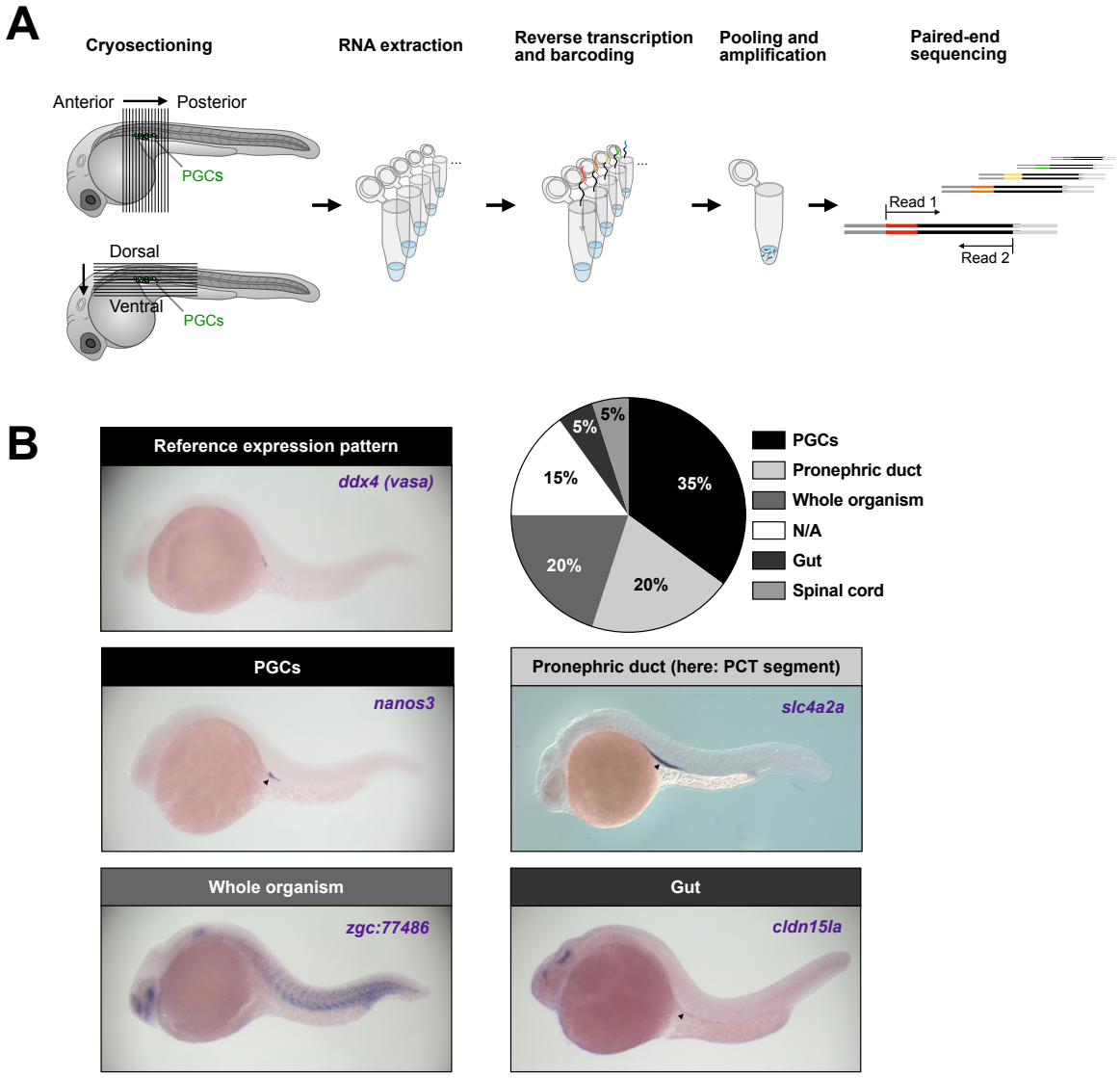

Fig. S1. RNA tomography identifies the pronephric duct as a structure adjacent to the PGCs. A. Schematic of the experimental setup. Embryos at 24 hpf were sectioned along the anterior–posterior and dorsal–ventral body axes to fully cover the gonadal ridge, where PGCs are located at this stage. RNA from individual sections was extracted, barcoded, and used for paired-end sequencing library preparation. **B.** Genes were ranked by the similarity of their expression profiles to the germ cell marker *ddx4* (formerly *vasa*) using Euclidean distance analysis. The 20 top ranking (most similar) genes were grouped according to the anatomical structures in which they are expressed, and the relative prevalence of these structures was compared. Representative whole-mount *in situ* hybridization images illustrate expression patterns in the respective tissues.

Development • Supplementary information

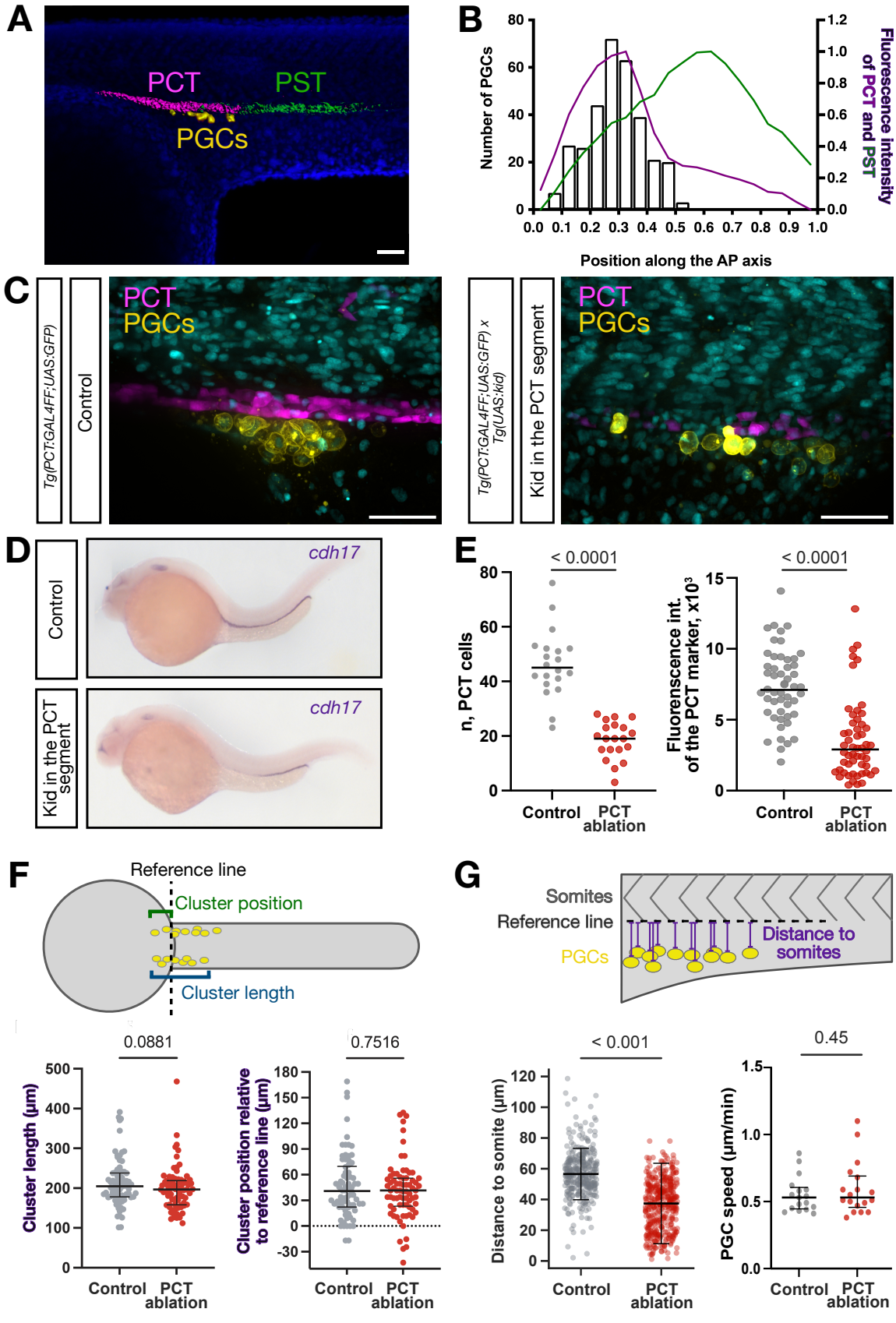

Development • Supplementary information

Fig. S2. PGC clustering upon arrival at the target region aligns with the proximal convoluted tubule region of the developing pronephric duct.
A-B. Quantification of the number of PGCs along the PCT and PST segments. **A.** PGCs were visualized with *Tg(kop:EGFP.F')* and an antisense probe for *egfp* mRNA. The PCT and PST segments were labeled using antisense probes for *nrip2* and *trpm7* mRNAs, respectively. Scale bar: 50 μm. **B.** The left y-axis shows the number of PGCs along the two segments. The right y-axis shows the fluorescence intensity of the PCT and PST markers. The x-axis shows the position of PGCs along the PCT and PST segments (as defined by the intensity profiles); here, 0 is the beginning of the PCT segment and 1 is the end of the PST segment. N = 25 embryos and n = 233 PGCs. The analysis was performed at 28 hpf. **C.** A 28 hpf control embryo expressing GFP in the PCT segment (left panel, magenta); a 28 hpf embryo expressing Kid and GFP in the PCT segment indicating significant loss of GFP within the PCT (right panel, magenta). All nuclei are expressing BFP (cyan) and germ cells are expressing farnesylated mCherry (yellow). Scale bar: 50 μm. **D.** mRNA expression pattern of *cdh17* (by WMISH) in control embryos (a representative embryo, left panel) and embryos expressing Kid in their PCT segment at 32 hpf (right panel). 80% of embryos that expressed Kid in the PCT showed a loss of *cdh17* expression in the PCT segment (a representative embryo in the right panel). **E**. Quantification of the PCT ablation by counting the number of the PCT cells (left graph, cells are presented in magenta in the panel **C,** N = 20 embryos for the control and N = 20 embryos analyzed for the PCT ablation) and by measuring mean fluorescent intensity (GFP channel) of the PCT marker (right graph, magenta in the panel **C,** N = 51 embryos for the control and N = 54 embryos analyzed for the PCT ablation). P – Student's t-test, error bars – IQR. Representative images for this experiment are shown in the panel **C**. **F-G.** Illustration of an embryo from the dorsal (**F**) and lateral (**G**) sides depicting the clusters of PGCs (yellow circles). Control embryos (*Tg(PCT:GAL4;UAS:GFP);Tg(kop:lifeact-mCherry)*) and embryos expressing Kid in the PCT (*Tg(PCT:GAL4;UAS:GFP);Tg(kop:lifeact-mCherry);Tg(UAS:kid)*) were assessed for cluster length (**F**, blue line), cluster position (**F**, green line) as well as for the dorso-ventral positioning of the PGCs (**G**, violet lines). For this analysis, we only used embryos that had at least 20% loss of GFP expression within the PCT segment compared to the average GFP intensity within control embryos. **F.** The position of the cluster (green line) was determined by

Development • Supplementary information

the distance from the most anterior PGC to a reference line (dotted line drawn at the cross section of the yolk and the trunk). N = 37 embryos and n = 74 PGC clusters for both control and Kid-expressing embryos. P – Student's t-test, error bars – IQR. **G**. The dorso-ventral positioning of the PGC cluster (left graph) was assessed by measuring the distance (violet lines) to germ cells from the closest ventral somites' border (dotted line). PCT ablation significantly reduced the distance of PGCs from the ventral somite border compared to control (Mann-Whitney U; $p = 6.05e^{-6}$). For statistical analysis, n = 30 PGCs were randomly sampled from each group. Black horizontal lines indicate median distances. Error bars: IQR; N = 52 embryos, n = 341 PGCs for control and N = 62 embryos, n = 397 PGCs for Kid-expressing embryos. Scale bar – 50 μm. Mean PGC speed in control and PCT-ablated embryos (right graph) was calculated from 60 min tracks from 10x time-lapse movies. N = 6 embryos, n = 17 PGCs for control and N = 6 embryos, n = 18 PGCs for the PCT ablation conditions. P – Student's t-test, error bars – IQR. Representative images for this experiment are shown in the panel **C**.

Development • Supplementary information

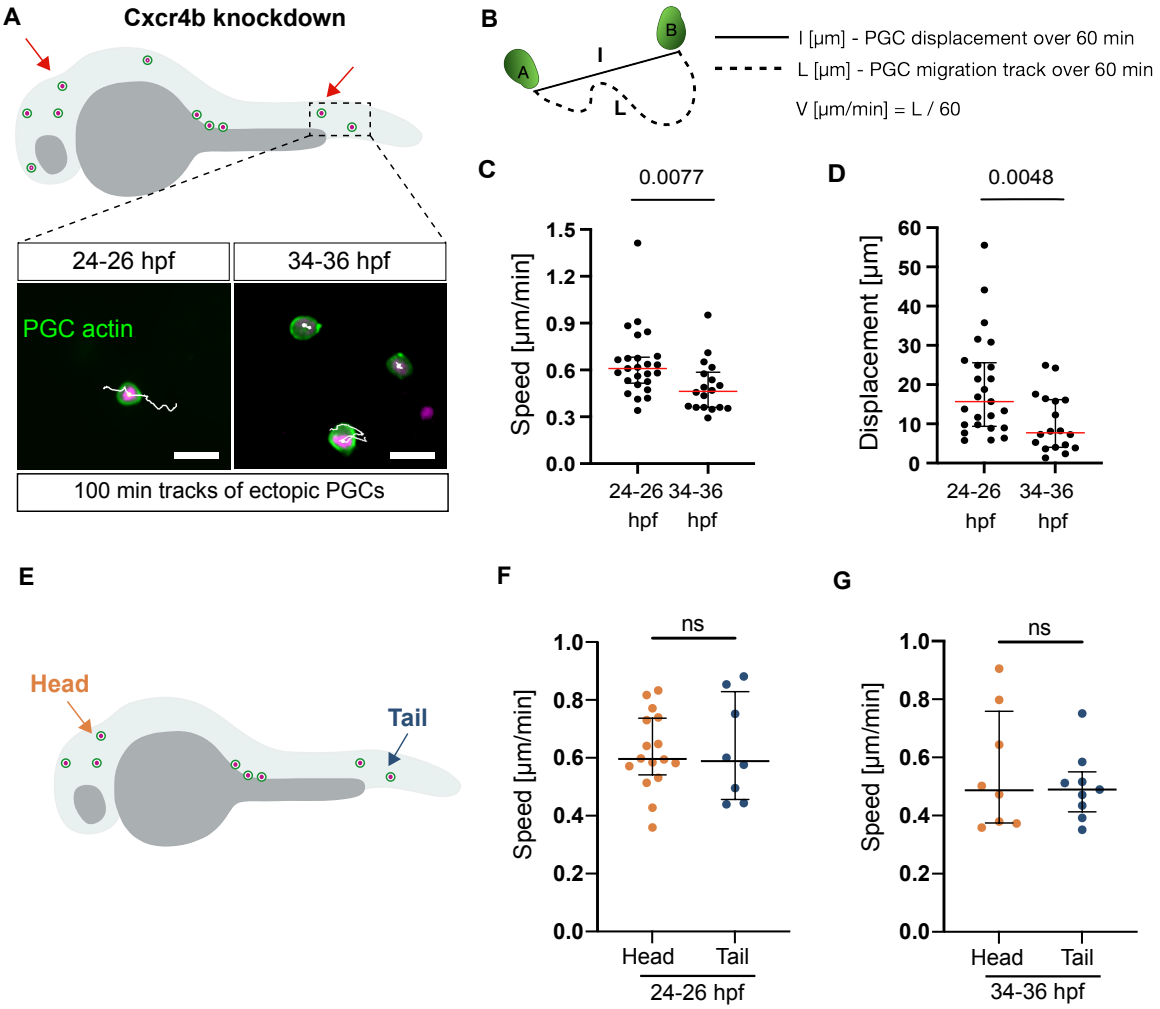

Fig. S3. PGCs' migration speed decay is not due to clustering.

A. Zebrafish embryo schematic with single PGCs located at ectopic regions such as the head and the tail as indicated by the red arrows. The associated images show magnified views of the regions marked by the dotted box, presenting tracks of PGC migration at an ectopic location (e.g., tail region) at 24-26 hpf (left panel) and at 34-36 hpf (right panel). PGCs were labeled by injecting a nuclear RFP-encoding mRNA into *Tg(kop:lifeact-EGFP)* embryos at the one-cell stage. Scale bar – 20 µm. **B.** Scheme illustrating calculation of PGC speed and displacement. Both parameters were calculated from 60 min PGC tracks. Displacement (I) is defined as the minimal distance (in µm) between starting (A) and final (B) PGC positions travelled by the cells during 1 h. Speed (V) is calculated by dividing the entire travel distance (L) over time (60 min). **C.** Migration speed of the ectopic PGCs at 24-26 hpf and 34-36 hpf. **D.** Displacement of the ectopic PGCs at 24-26 hpf and 34-36 hpf. N = 15 embryos, n = 25 PGCs (24-26 hpf); N = 8 embryos, n = 18 PGCs (34-36 hpf). **E.** Zebrafish embryo

Development • Supplementary information

schematic with single PGCs located at ectopic regions such as the head (orange arrow) and the tail (blue arrow). **F-G.** Migration speed of ectopic PGCs located at the head versus migration speed of ectopic PGCs at the tail at 24-26 hpf (**F**) and at 34-36 hpf (**G**). For the head, N = 8, n = 16 PGCs (**F**); N = 6 embryos and n = 9 PGCs (**G**). For the tail, N = 7 embryos and n = 8 PGCs (**F**); N = 4 embryos and n = 9 PGCs (**G**). P – Student's t-test, error bars – IQR.

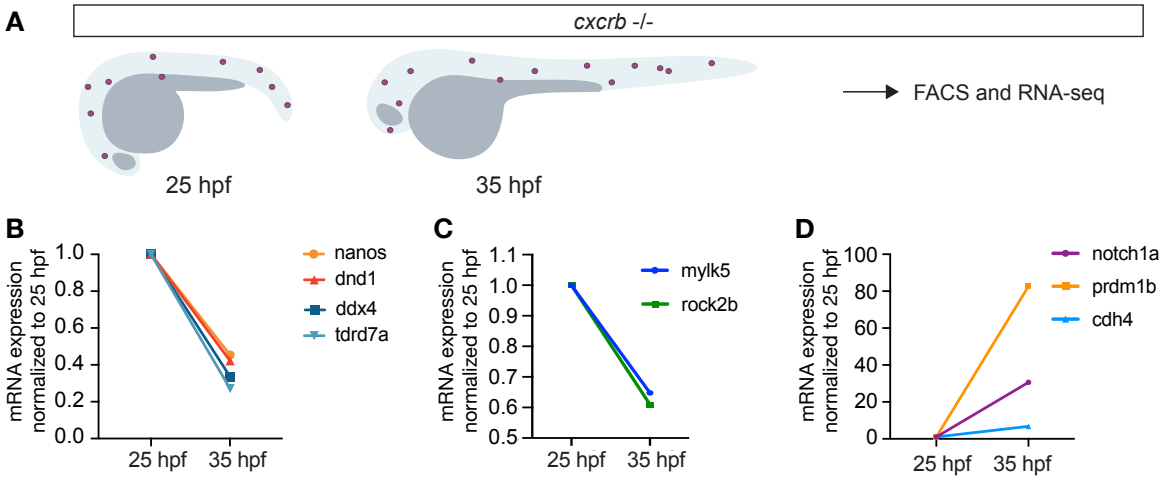

Fig. S4. mRNA levels of proteins important for PGC contractility, specification and differentiation change from 15 to 35 hpf. A. Illustration of 25 and 35 hpf *(cxcr4b$^{-/-}$;Tg(kop:mCherry.F'))* embryos used for FACS of PGCs (magenta) and subsequently for obtaining PGC-specific transcriptomes. The normalized mRNA levels of proteins important for specification of germ cells (**B**), for contractility and motility of PGCs (**C**), as well as for the differentiation and adhesion (**D**) are depicted at 25 and 35 hpf.

Development • Supplementary information

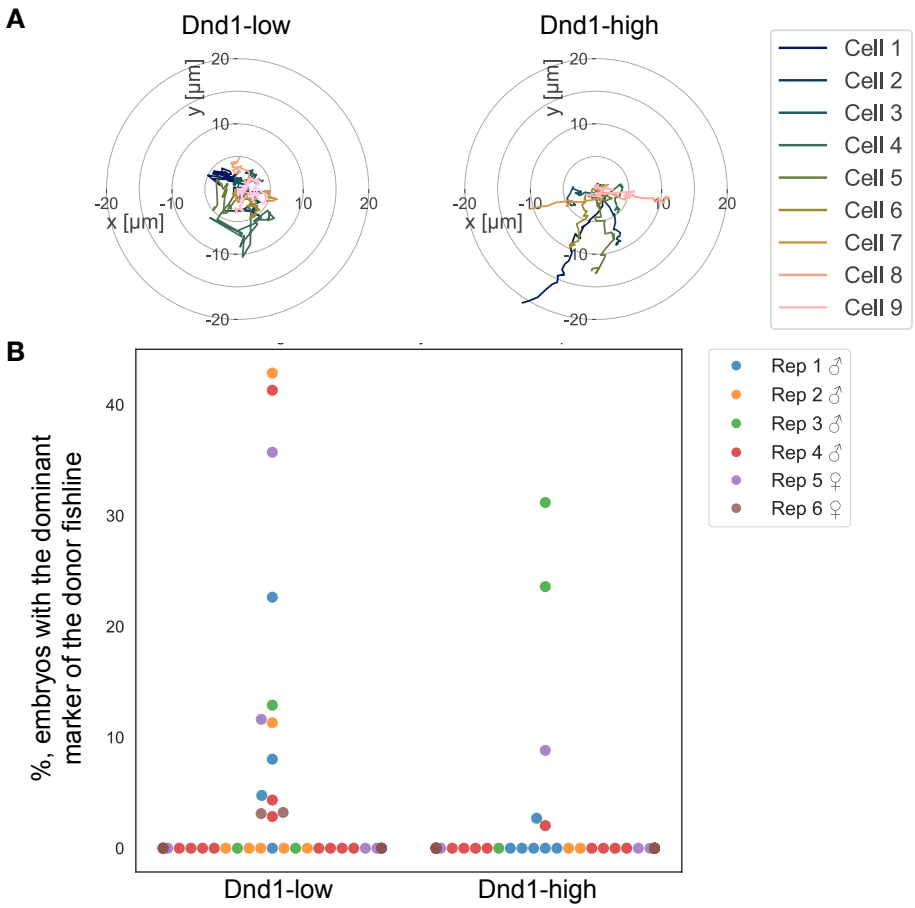

Fig. S5. Reduction of PGC motility at later developmental stages is dependent on the function of Dnd-1 and important for the germline transmission. A. Representative 60-minute tracks of migrating germ cells analyzed in (**Fig. 4B, C**). **B.** Germline transmission efficiency of the transplanted donor germ cells with either normal (Dnd1-low) or high (Dnd1-high) Dnd1 expression levels. Percentage of embryos with the dominant marker of the donor fishline in each offspring clutch from the experiment shown in Fig. 4D. Each dot represents the individual egg clutch of host fish outcross. Colored by replicates (N = 6 replicates; in total 51 males ♂ and 34 females♀ analyzed).

Development • Supplementary information

Table S1. RNA-tomography results: Transcripts with expression patterns most similar to *ddx4/vasa*

	Gene	Distance to vasa (24 hpf)	Expression (24 hpf)	Cell Type / Tissue
1	vasa'	0.00	23.21	germ cell
2	'ca15b'	2.18	18.84	germ cell
3	'dnd1'	2.45	21.88	germ cell
4	'nanos3'	2.96	145.98	germ cell
5	'dazl'	3.15	12.32	germ cell
6	'tdrd7a'	3.87	4.40	germ cell
7	'h1m'	4.14	24.46	germ cell
8	'tspan13a'	4.39	55.32	other
9	si:dkey-71l4.5'	4.45	4.01	other
10	'cldn15la'	4.54	13.52	gut
11	'nostrin'	4.55	14.34	whole organism
12	si:rp71-17i16.6'	4.58	19.99	other
13	ogal'	4.99	7.21	other
14	'cfd'	5.07	311.67	pronephric duct, epidermis
15	'TMEM235'	5.11	10.36	other
16	slc4a2a'	5.17	442.71	pronephric duct, PCT
17	slc9a3r1a'	5.20	95.01	pronephric duct
18	slc5a9'	5.20	22.89	pronephric duct, PCT
19	grasp'	5.24	20.89	whole organism
20	zgc:77486'	5.25	13.00	other

Development • Supplementary information

Table S2. Fishlines employed in this work

Fishline (internal name)	Reference
Wild-type strain of the AB or ABxTL background (WT)	
Tg(kop:EGFP.F'.nos3'UTR-cry: dsRed) (24)	(Blaser et al., 2006)
Tg(kop:lifeact-EGFP.nos3'UTR-cry: dsRed) (38)	(Hartwig et al., 2014)
Cxcr4b ^{t26035} *(ody)*	(Knaut et al., 2003)
Spadetail (Spt ^{b104}*)*	(Ho and Kane, 1990)
Tg(kop:YPet.Ezrin.nos3'UTR.cmlc:EGFP)/ Tg(kop:lifeact-mCherry.nos3'UTR-cry:dsRed) (99/118)	(Olguin-Olguin et al., 2021)
Tg(kop:mCherry.F'.nos3'UTR-cmlc:EGFP) (57)	(Tarbashevich et al., 2015)
Tg(vasa:vasa-EGFP) (81)	(Krøvel and Olsen, 2002)
Tg(buc:buc-EGFP) (180)	(Riemer et al., 2015)
Tg(PCT:GAL4FF;UAS:GFP)/ gSALzGFFD397A (186)	(Kawakami et al., 2010)
Tg(UAS:kid;cmlc:EGFP) (222)	(Labbaf et al., 2022)

Development • Supplementary information

Table S3. DNA constructs employed in this work

Construct	Internal DB number	Reference
mCherry-h2b.globin3'utr	**B325**	(Paksa et al., 2016)
tdTomato-nls.nos3'utr	**C863**	(Olguin-Olguin et al., 2021)
h2a-tagbfp.SV40polyA	**D846**	(Compagnon et al., 2014)
dnd1.globin3'utr	**487**	(Weidinger et al., 2003)
vasaFL.globin3'utr	**333**	(Köprunner et al., 2001)
pCS2-buc	**B639**	(Riemer et al., 2015)
tdrd6.globin3'utr	**F089**	(Hoffmann et al., 2025)
tdrd7.globin3'utr	**A241**	(Hoffmann et al., 2025)
nanos3CDS.globin3'utr	**278**	(Köprunner et al., 2001)
mGFP.nos3'utr	**355**	(Köprunner et al., 2001)

Development • Supplementary information

Supplementary References

Blaser, H., Reichman-Fried, M., Castanon, I., Dumstrei, K., Marlow, F. L., Kawakami, K., Solnica-Krezel, L., Heisenberg, C.-P. and Raz, E. (2006). Migration of Zebrafish Primordial Germ Cells: A Role for Myosin Contraction and Cytoplasmic Flow. *Developmental Cell* 11, 613–627.

Compagnon, J., Barone, V., Rajshekar, S., Kottmeier, R., Pranjic-Ferscha, K., Behrndt, M. and Heisenberg, C.-P. (2014). The Notochord Breaks Bilateral Symmetry by Controlling Cell Shapes in the Zebrafish Laterality Organ. *Developmental Cell* 31, 774–783.

Cunningham, F., Achuthan, P., Akanni, W., Allen, J., Amode, M. R., Armean, I. M., Bennett, R., Bhai, J., Billis, K., Boddu, S., et al. (2019). Ensembl 2019. *Nucleic Acids Research* 47, D745–D751.

Dobin, A., Davis, C. A., Schlesinger, F., Drenkow, J., Zaleski, C., Jha, S., Batut, P., Chaisson, M. and Gingeras, T. R. (2013). STAR: ultrafast universal RNA-seq aligner. *Bioinformatics* 29, 15–21.

Hartwig, J., Tarbashevich, K., Seggewiß, J., Stehling, M., Bandemer, J., Grimaldi, C., Paksa, A., Groß-Thebing, T., Meyen, D. and Raz, E. (2014). Temporal control over the initiation of cell motility by a regulator of G-protein signaling. *Proc. Natl. Acad. Sci. U.S.A.* 111, 11389–11394.

Hashimshony, T., Wagner, F., Sher, N. and Yanai, I. (2012). CEL-Seq: Single-Cell RNA-Seq by Multiplexed Linear Amplification. *Cell Reports* 2, 666–673.

Ho, R. K. and Kane, D. A. (1990). Cell-autonomous action of zebrafish spt-1 mutation in specific mesodermal precursors. *Nature* 348, 728–730.

Hoffmann, D., Agranov, T., Kühl, L., Ermlich, L., Reichman-Fried, M., Simons, B. D., Gov, N. S. and Raz, E. (2025). Corrections in single-cell migration path in vivo are controlled by pulses in polar Rac1 activation. *Current Biology* 35, 4365-4382.e8.

Kawakami, K., Abe, G., Asada, T., Asakawa, K., Fukuda, R., Ito, A., Lal, P., Mouri, N., Muto, A., Suster, M. L., et al. (2010). zTrap: zebrafish gene trap and enhancer trap database. *BMC Dev Biol* 10, 105.

Köprunner, M., Thisse, C., Thisse, B. and Raz, E. (2001). A zebrafish *nanos* -related gene is essential for the development of primordial germ cells. *Genes Dev.* 15, 2877–2885.

Krøvel, A. V. and Olsen, L. C. (2002). Expression of a vas::EGFP transgene in primordial germ cells of the zebrafish. *Mechanisms of Development* 116, 141–150.

Development • Supplementary information

Labbaf, Z., Petratou, K., Ermlich, L., Backer, W., Tarbashevich, K., Reichman-Fried, M., Luschnig, S., Schulte-Merker, S. and Raz, E. (2022). A robust and tunable system for targeted cell ablation in developing embryos. *Developmental Cell* 57, 2026-2040.e5.

Olguin-Olguin, A., Aalto, A., Maugis, B., Boquet-Pujadas, A., Hoffmann, D., Ermlich, L., Betz, T., Gov, N. S., Reichman-Fried, M. and Raz, E. (2021). Chemokine-biased robust self-organizing polarization of migrating cells in vivo. *Proc. Natl. Acad. Sci. U.S.A.* 118, e2018480118.

Paksa, A., Bandemer, J., Hoeckendorf, B., Razin, N., Tarbashevich, K., Minina, S., Meyen, D., Biundo, A., Leidel, S. A., Peyrieras, N., et al. (2016). Repulsive cues combined with physical barriers and cell–cell adhesion determine progenitor cell positioning during organogenesis. *Nat Commun* 7, 11288.

Patro, R., Duggal, G., Love, M. I., Irizarry, R. A. and Kingsford, C. (2017). Salmon provides fast and bias-aware quantification of transcript expression. *Nat Methods* 14, 417–419.

Riemer, S., Bontems, F., Krishnakumar, P., Gömann, J. and Dosch, R. (2015). A functional Bucky ball-GFP transgene visualizes germ plasm in living zebrafish. *Gene Expression Patterns* 18, 44–52.

Tarbashevich, K., Reichman-Fried, M., Grimaldi, C. and Raz, E. (2015). Chemokine-Dependent pH Elevation at the Cell Front Sustains Polarity in Directionally Migrating Zebrafish Germ Cells. *Current Biology* 25, 1096–1103.

Tarbashevich, K., Ermlich, L., Wegner, J., Pfeiffer, J. and Raz, E. (2023). The mitochondrial protein Sod2 is important for the migration, maintenance, and fitness of germ cells. *Front. Cell Dev. Biol.* 11, 1250643.

Weidinger, G., Stebler, J., Slanchev, K., Dumstrei, K., Wise, C., Lovell-Badge, R., Thisse, C., Thisse, B. and Raz, E. (2003). dead end, a Novel Vertebrate Germ Plasm Component, Is Required for Zebrafish Primordial Germ Cell Migration and Survival. *Current Biology* 13, 1429–1434.

the distance from the most anterior PGC to a reference line (dotted line drawn at the cross section of the yolk and the trunk). N = 37 embryos and n = 74 PGC clusters for both control and Kid-expressing embryos. P – Student's t-test, error bars – IQR. **G**. The dorso-ventral positioning of the PGC cluster (left graph) was assessed by measuring the distance (violet lines) to germ cells from the closest ventral somites' border (dotted line). PCT ablation significantly reduced the distance of PGCs from the ventral somite border compared to control (Mann-Whitney U; $p = 6.05e^{-6}$). For statistical analysis, n = 30 PGCs were randomly sampled from each group. Black horizontal lines indicate median distances. Error bars: IQR; N = 52 embryos, n = 341 PGCs for control and N = 62 embryos, n = 397 PGCs for Kid-expressing embryos. Scale bar – 50 μm. Mean PGC speed in control and PCT-ablated embryos (right graph) was calculated from 60 min tracks from 10x time-lapse movies. N = 6 embryos, n = 17 PGCs for control and N = 6 embryos, n = 18 PGCs for the PCT ablation conditions. P – Student's t-test, error bars – IQR. Representative images for this experiment are shown in the panel **C**.

Development • Supplementary information

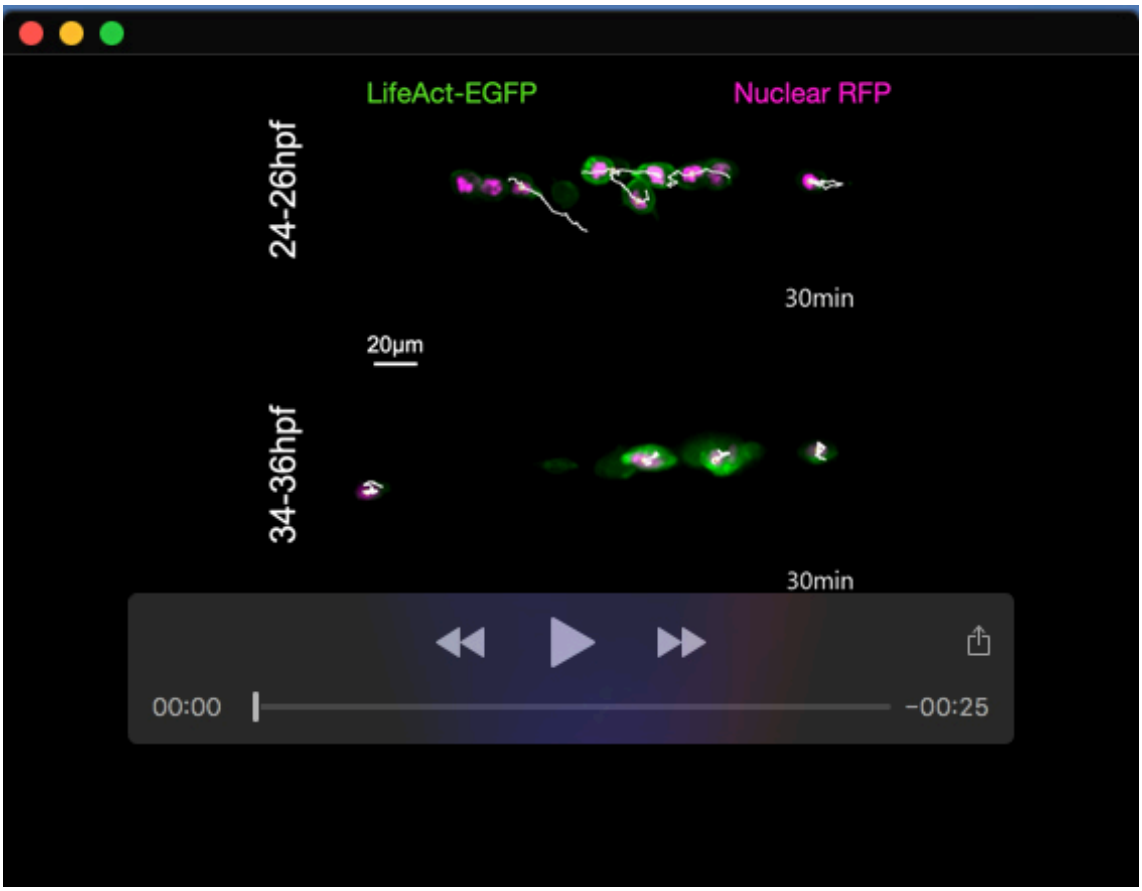

Movie 1. Germ cell migration speed is reduced during development. Time-lapse imaging of PGCs at the gonad region at 24-26 hpf (upper half) and at 34-36 hpf (lower half). PGCs were labeled by injecting nuclear tdTomato-encoding mRNA in *Tg(kop:lifeact-EGFP)* embryos at the one-cell stage.

Development • Supplementary information